RESEARCH MEMORANDUM

STABILITY CHARACTERISTICS AT LOW SPEED OF A $\frac{1}{4}$-SCALE BELL X-5 AIRPLANE MODEL WITH VARIOUS MODIFICATIONS TO THE BASIC MODEL CONFIGURATIONS

By Robert E. Becht and Albert G. Few, Jr.

Langley Aeronautical Laboratory
Langley Air Force Base, Va.

NATIONAL ADVISORY COMMITTEE
FOR AERONAUTICS

WASHINGTON
August 16, 1950

NATIONAL ADVISORY COMMITTEE FOR AERONAUTICS

RESEARCH MEMORANDUM

STABILITY CHARACTERISTICS AT LOW SPEED OF A $\frac{1}{4}$ - SCALE BELL X-5 AIRPLANE MODEL WITH VARIOUS MODIFICATIONS TO THE BASIC MODEL CONFIGURATIONS

By Robert E. Becht and Albert G. Few, Jr.

SUMMARY

An investigation was made of the low-speed longitudinal, lateral, and directional stability characteristics of a $\frac{1}{4}$ - scale model of a preliminary Bell X-5 airplane design with various modifications to the basic model configuration. The extended dive brakes increased the drag coefficient at low lifts about 0.02 for both 20° and 60° wing-sweep configurations and produced a destabilizing shift in the aerodynamic center of the complete model of the order of 2 and 7 percent of the wing mean aerodynamic chord at 50° sweep for 20° and 60° sweep, respectively. No significant changes in the longitudinal, lateral, or directional stability of the model were obtained by adding wing trailing-edge fillets. Increasing the wing aspect ratio of the 60° configuration from 1.92 to 2.25 resulted in a decrease in the longitudinal stability at high lift coefficients. None of the modifications which were made primarily in an attempt to improve directional stability at high lift coefficients with 60° sweep were successful in eliminating the rapid variation of directional stability with lift coefficient near the stall.

INTRODUCTION

An investigation of the stability and control characteristics of a $\frac{1}{4}$ - scale model of a preliminary Bell X-5 airplane design has been conducted in the Langley 300 MPH 7- by 10-foot wind tunnel at a Mach number of 0.152 and a Reynolds number of 2,000,000. The Bell X-5 airplane is a proposed research airplane incorporating wings whose sweepback angle can be varied continuously between 20° and 60°. Provision for longitudinal translation of the wing with respect to the fuselage is also made.

The results of the longitudinal stability and control investigation of the basic model configuration are presented in reference 1. The results of the lateral and directional stability and control investigation of the basic model configuration are presented in reference 2. This paper contains the results of additional studies of the longitudinal, lateral, and directional stability characteristics of the model at sweep angles of 20° and 60°. The purpose of the investigation was twofold: (1) to determine the effect of dive brakes and contemplated design changes in the wing plan form of the airplane and (2) to determine whether any improvement in the poor directional stability of the 60° configuration at high lift coefficients would be realized by the addition of wing fences, changes in wing incidence, or by use of various fuselage fin arrangements. (See reference 2.)

SYMBOLS

The system of axes employed, together with an indication of the positive direction of the forces, moments, and angles, is presented in figure 1. The symbols used in this paper are defined as follows:

C_L	lift coefficient (Lift/qS)
C_X	longitudinal-force coefficient (X/qS)
C_{D_o}	$-C_X$ at $C_L = 0$
C_Y	lateral-force coefficient (Y/qS)
C_l	rolling-moment coefficient (L/qSb)
C_m	pitching-moment coefficient $\left(M/qS\bar{c}_{50}\right)$
C_n	yawing-moment coefficient (N/qSb)
X	longitudinal force along X-axis (Drag = -X), pounds
Y	lateral force along Y-axis, pounds
Z	force along Z-axis (Lift = -Z), pounds
L	rolling moment about X-axis, foot-pounds
M	pitching moment about Y-axis, foot-pounds

N	yawing moment about Z-axis, foot-pounds
q	free-stream dynamic pressure, pounds per square foot $\left(\frac{\rho V^2}{2}\right)$
S	wing area, square feet
$\bar{c}$	wing mean aerodynamic chord, feet (based on wing plan form as shown in fig. 2)
$\bar{c}_{50}$	wing mean aerodynamic chord at 50° sweep, feet
b	wing span, feet
V	free-stream velocity, feet per second
A	aspect ratio (b^2/S)
ρ	mass density of air, slugs per cubic foot
α	angle of attack of thrust line, degrees
ψ	angle of yaw, degrees
i_t	angle of incidence of stabilizer with respect to thrust line, degrees
i_w	angle of incidence of wing chord line with respect to thrust line, degrees
Λ	angle of sweepback of quarter-chord line of unswept wing, degrees

Subscript:

ψ	denotes partial derivative of a coefficient with respect to yaw $\left(\text{example: } C_{l_\psi} = \frac{\partial C_l}{\partial \psi}\right)$

APPARATUS AND METHODS

Description of Model

The model used in this investigation was a $\frac{1}{4}$-scale model of a preliminary Bell X-5 airplane design and must, therefore, be considered only qualitatively representative of the X-5 airplane.

Physical characteristics of the model are presented in figure 2 and a photograph of the model on the support strut is given in figure 3. Details of the dive brakes, trailing-edge fillets, and extended wing tips are presented in figure 4. Details of the wing fence and 5° increased wing incidence are presented in figure 5 and several fuselage fin arrangements in figure 6. The 20° drooped horizontal tail also shown in figure 6 has the same geometric characteristics as the horizontal tail shown in figure 2. The model was constructed of wood bonded to steel reinforcing members.

The wings were pivoted about an axis normal to the wing chord plane. Thus, the original wing incidence measured in a streamwise direction was zero for all sweep angles. At all sweep angles, the wing was located so that the quarter chord of the mean aerodynamic chord fell on a fixed fuselage station. The moment reference center was located at this fuselage station unless otherwise stated. (See fig. 2.)

The jet-engine ducting was simulated on the model by the use of an open tube having an inside diameter equal to that of the jet exit and extending from the nose to the jet exit.

Tests

The tests were conducted in the Langley 300 MPH 7- by 10-foot wind tunnel at a dynamic pressure of 34.15 pounds per square foot which corresponds to a Mach number of 0.152 and a Reynolds number of 2,000,000 based on the mean aerodynamic chord of the wing at 50° sweep for average test conditions.

During the tests no control was imposed on the quantity of air flow through the jet duct. Measurements made in subsequent tests indicated that the inlet velocity ratio varied between 0.78 and 0.86, the higher values being observed at low angles of attack.

Two types of tests were employed for determining the lateral characteristics of the model. The parameters C_{n_ψ}, C_{Y_ψ}, and C_{l_ψ} were determined from tests through the angle-of-attack range at yaw angles of 0° and 5°. The lateral characteristics were also determined from tests through a range of yaw angles at constant angle of attack.

Corrections

The angle-of-attack, drag, and pitching-moment results have been corrected for jet-boundary effects computed on the basis of unswept wings by the methods of reference 3. Independent calculations have shown that the effects of sweep on the above corrections are negligible. All coefficients have been corrected for blocking by the model and its wake by the method of reference 4.

Corrections for the tare forces and moments produced by the support strut have not been applied. It is probable, however, that the significant tare corrections would be limited to small increments in pitching moment and drag.

Buoyancy effects on the support strut, tunnel air-flow misalinement, and longitudinal pressure gradient have been accounted for in computation of the test data.

RESULTS AND DISCUSSION

Presentation of Results

The longitudinal aerodynamic characteristics of the basic model configuration with 20° and 60° wing sweep are presented in figures 7(a) and 7(b), respectively. These data are taken from reference 1 and are repeated here to allow for comparison with the longitudinal aerodynamic characteristics of the model with the various modifications. Figure 7(a) shows that some discrepancies exist between the two sets of data for the $-\frac{3}{4}^\circ$ stabilizer setting with the greatest discrepancies occurring mainly at high lift coefficients. These discrepancies are believed to be caused primarily by small inaccuracies in setting the slat in its retracted position, thus producing changes in the wing leading-edge contour. It is believed that the flagged rather than the unflagged symbols in figure 7(a) represent more closely the condition of the wing leading edge during tests of the modifications discussed below. Care should be exercised in evaluating the effect on maximum lift coefficient of the modifications to be presented.

The principal results of the investigation are presented in the figures summarized below:

The aerodynamic coefficients presented herein are based on the wing area and span of the sweep in question and on the mean aerodynamic chord of the wing at 50° sweep. Thus, the pitching-moment coefficients are based on a reference length which is fixed in the fuselage and is independent of the sweep angle whereas all other coefficients are of the usual form.

Dive Brakes

When the dive brakes were extended, an increase in drag coefficient at low lift coefficients of the order of 0.02 was realized for both 20° and 60° sweep configurations. (See figs. 7(a) and 8(a), and 7(b) and 8(b).) A destabilizing shift of the aerodynamic center $\left(\frac{\partial C_m}{\partial C_L}\right)_{Tail}$ on of the order of $0.02\bar{c}_{50}$ at 20° sweep and $0.07\bar{c}_{50}$ at 60° sweep occurred when the dive brakes were extended although essentially no change in lift-curve slope was noted. A nose-down trim change at low lift coefficients was also noted for both sweep configurations.

When the dive brakes were extended, a reduction in directional stability occurred at high lift coefficients in the 20° wing-sweep configuration. Directional-stability reductions were also experienced

from $C_L \approx 0.1$ over the lift-coefficient range in the 60° sweep configuration with dive brakes extended.

Trailing-Edge Fillets

The contemplated X-5 wing construction leaves a large cutout at the wing-root trailing-edge juncture with the fuselage when low wing-sweep angles are used. An investigation was made with the cutout covered by an upper-surface fillet of the plan form shown in figure 4 to determine the effect on the stability characteristics of the model. Inasmuch as the entire fillet lies on the wing surface at high wing-sweep angles, tests were made at only 20° sweep and the coefficients computed by using the basic wing area.

A comparison of the data in figures 7(a) and 11 indicates a slight rearward shift of the wing-fuselage aerodynamic center and a slight increase in negative pitching-moment coefficient at zero lift probably as a result of the added fillet area rearward of the wing trailing edge. The longitudinal stability of the model, however, remained essentially unchanged inasmuch as the increase in downwash at the tail apparently compensated for the wing-fuselage aerodynamic-center shift.

The addition of the trailing-edge fillet also produced slight increases in lift-curve slope and minimum drag. The directional stability remained essentially unchanged but slight reductions were obtained in the effective dihedral at low lift coefficients (fig. 12).

Extended Wing Tips

One of the preliminary X-5 airplane designs incorporated a wing of higher aspect ratio than that on the model. As a means of evaluating this aspect-ratio change in terms of test model characteristics, the aspect ratio of the model wing was increased to that of the airplane design by extending the wing tips as shown in figure 4. Since an increase in aspect ratio would be expected to have a more critical effect on longitudinal stability at high wing-sweep angles, the investigation was limited to the one wing-sweep angle of 60°. The wing pivot points had the same location with respect to the fuselage as in previous 60° wing-sweep configurations but the moment reference center was shifted rearward 1.75 inches as a result of the new mean-aerodynamic-chord location. All force and moment coefficients were calculated in a manner previously outlined with $\bar{c}_{50}$ computed as 1.931 feet.

It can be seen in figure 14 that the higher-aspect-ratio wing produced an undesirable decrease in stability at lift coefficients above 0.65, resulting in a change in stability throughout the lift

range of considerably greater magnitude than that encountered with the basic plan form. Other longitudinal aerodynamic characteristics of the test model were essentially unchanged by the addition of the extended wing tips.

The directional stability was decreased somewhat although instability was indicated at about the same lift coefficient for both model configurations. (See fig. 15.) Changes in the effective dihedral were limited to the high-lift-coefficient range where the extended-wing-tip configuration had somewhat higher values than the basic model. The lift-coefficient value at which zero effective dihedral was obtained was increased about 0.22 where the higher aspect ratio wing was used.

Fences

Examination of the longitudinal characteristics of the model with 60° sweep together with tuft observations of the flow on the wing led to the conclusion that the flow around the 60° swept wing at high lift coefficients was dominated by the action of a leading-edge separation vortex which contributed to the strong spanwise velocity components in the boundary layer and flow separation over the regions of the wing near the tip. It was anticipated that an upper-surface fence might divert the course of this vortex flow and thus alter the spanwise progression of flow separation. A full-chord fence was installed on the model as shown on figure 5 to determine whether or not the resulting changes in direct forces on the wing and in flow direction at the tail would be beneficial to the directional stability at high lift coefficients. The effects of adding the fences are shown in figures 17 and 18.

Figure 17 indicates that the fence produced an undesirable region of reduced longitudinal stability at lift coefficients near 0.8. The reduction in the nonlinearities of the lift curve above $C_L \approx 0.3$ resulted in less lift at a given angle of attack for the model with the fence than for the basic configuration. A slight increase in drag, particularly at the higher lift coefficients can also be noted as a result of the increased angle of attack required to produce a given lift coefficient.

Figure 18 shows that the fence produced essentially no improvement in the undesirable directional stability characteristics near the stall. The rate of increase of C_{n_ψ} with lift coefficient at high lift coefficients for the original configuration, however, is so great that any modification to the model would have to produce an extremely large reduction in C_{n_ψ} at high lift coefficients in order to result in any significant gain in the lift coefficient at which directional instability occurred. The addition of the fence did not change the lift

coefficient at which the model became directionally unstable. The lift coefficient at which zero effective dihedral occurred was increased about 0.22 when the fence was added.

Wing Incidence

Figure 18 of reference 2 indicates that the directional stability of the fuselage-tail configuration decreased rapidly with increasing angle of attack. Increased wing incidence was investigated in an attempt to improve the directional stability characteristics by reducing the fuselage angle of attack corresponding to a given lift coefficient. The results of the investigation are presented in figures 19 and 20.

Figure 19 shows that the increased wing incidence had no effect on longitudinal stability at low lift coefficients. Above a lift coefficient of 0.65, however, the model became unstable and continued so until just before stall, probably as a result of the tail being raised relative to the wing so that the tail was placed in a region where downwash characteristics differ from those of the basic configuration. The decrease in lift-curve slope above $C_L \approx 0.65$ and the reduction in $C_{L_{max}}$ probably also result from the downwash change at the tail. Slightly higher drag, especially at higher lift coefficients, was also obtained.

The directional stability of the original model configuration at 60° sweep decreased rapidly at the higher lift coefficients becoming unstable at a value of lift coefficient about 0.2 below $C_{L_{max}}$. With the change in wing incidence, directional instability occurred only 0.08 below $C_{L_{max}}$ but the value of $C_{L_{max}}$ was reduced to such an extent that there was no net increase in the lift coefficient at which directional instability occurred. (See fig. 20.) At lift coefficients below 1.1, the incidence change affected the sidewash at the tail enough to result in some increase in directional stability, particularly in the low-lift-coefficient range. The increase in C_{Y_ψ} at low lift coefficients is almost directly reflected in the increase in directional stability and increased dihedral effect. These effects at low lift coefficients are obtained at the expense of the loss in longitudinal stability at higher lift coefficients, the reduction in $C_{L_{max}}$, and the reduction in effective dihedral at lift coefficients above 0.82.

Fins

Flow surveys in the vicinity of the vertical tail indicated that the directional instability at high lift coefficients was associated with the presence of a large vortex pattern that covered part of the tail when the model was yawed. Attempts were made to break up this formation by adding various fuselage, dorsal, and ventral fins as shown in figure 6. As a means of adding effective ventral area a drooped horizontal tail was also investigated. The lift-coefficient value at zero yaw at which the investigation was made was 1.1 for all fin arrangements. No significant improvements in either directional or lateral stability of the model were produced by any of the fin configurations. (See fig. 21.)

The several modifications investigated in an attempt to improve the directional stability at high lift coefficients at 60° sweep were not particularly beneficial. It is probable, however, that the directional instability encountered would not have serious adverse effects on the flight characteristics of the X-5 research airplane since landings at high sweep angles are not contemplated. For military designs, maneuvers requiring high lift coefficients at 60° sweep would be undesirable because of the high drag coefficients obtained.

CONCLUSIONS

An investigation at low speed of the effect on longitudinal, lateral, and directional stability of various modifications to the basic $\frac{1}{4}$-scale model of a preliminary Bell X-5 airplane design was made and the following conclusions are drawn:

1. The extended dive brakes increased the drag coefficient at low lifts about 0.02 for both 20° and 60° wing-sweep configurations and produced a destabilizing shift in the aerodynamic center of the order of 2 and 7 percent of the wing mean aerodynamic chord at 50° sweep for 20° and 60° sweep, respectively.

2. The addition of the trailing-edge fillets had no significant effect on the longitudinal, lateral, or directional stability.

3. Increasing the wing aspect ratio resulted in a decrease in longitudinal stability at high lift coefficients.

4. None of the modifications investigated primarily in an attempt to improve directional stability at high lift coefficients with 60° sweep were successful in eliminating the rapid variation of directional

stability with lift coefficient near the stall. Although changes were experienced at low lift coefficients, none of the modifications delayed the lift coefficient at which directional instability occurred. These modifications included the addition of a wing fence, increased wing incidence, and the addition of various dorsal, ventral, and fuselage side fins.

5. The lift coefficient at which zero effective dihedral was observed was increased about 0.22 when either the higher-aspect-ratio wing or the fence was used.

Langley Aeronautical Laboratory
National Advisory Committee for Aeronautics
Langley Air Force Base, Va.

REFERENCES

1. Kemp, William B., Jr., Becht, Robert E., and Few, Albert G., Jr.: Stability and Control Characteristics at Low Speed of a $\frac{1}{4}$-Scale Bell X-5 Airplane Model. Longitudinal Stability and Control. NACA RM L9K08, 1950.

2. Kemp, William B., Jr., and Becht, Robert E.: Stability and Control Characteristics at Low Speed of a $\frac{1}{4}$-Scale Bell X-5 Airplane Model. Lateral and Directional Stability and Control. NACA RM L50C17a, 1950.

3. Gillis, Clarence L., Polhamus, Edward C., and Gray, Joseph L., Jr.: Charts for Determining Jet-Boundary Corrections for Complete Models in 7- by 10-Foot Closed Rectangular Wind Tunnels. NACA ARR L5G31, 1945.

4. Herriot, John G.: Blockage Corrections for Three-Dimensional-Flow Closed-Throat Wind Tunnels, with Consideration of the Effect of Compressibility. NACA RM A7B28, 1947.

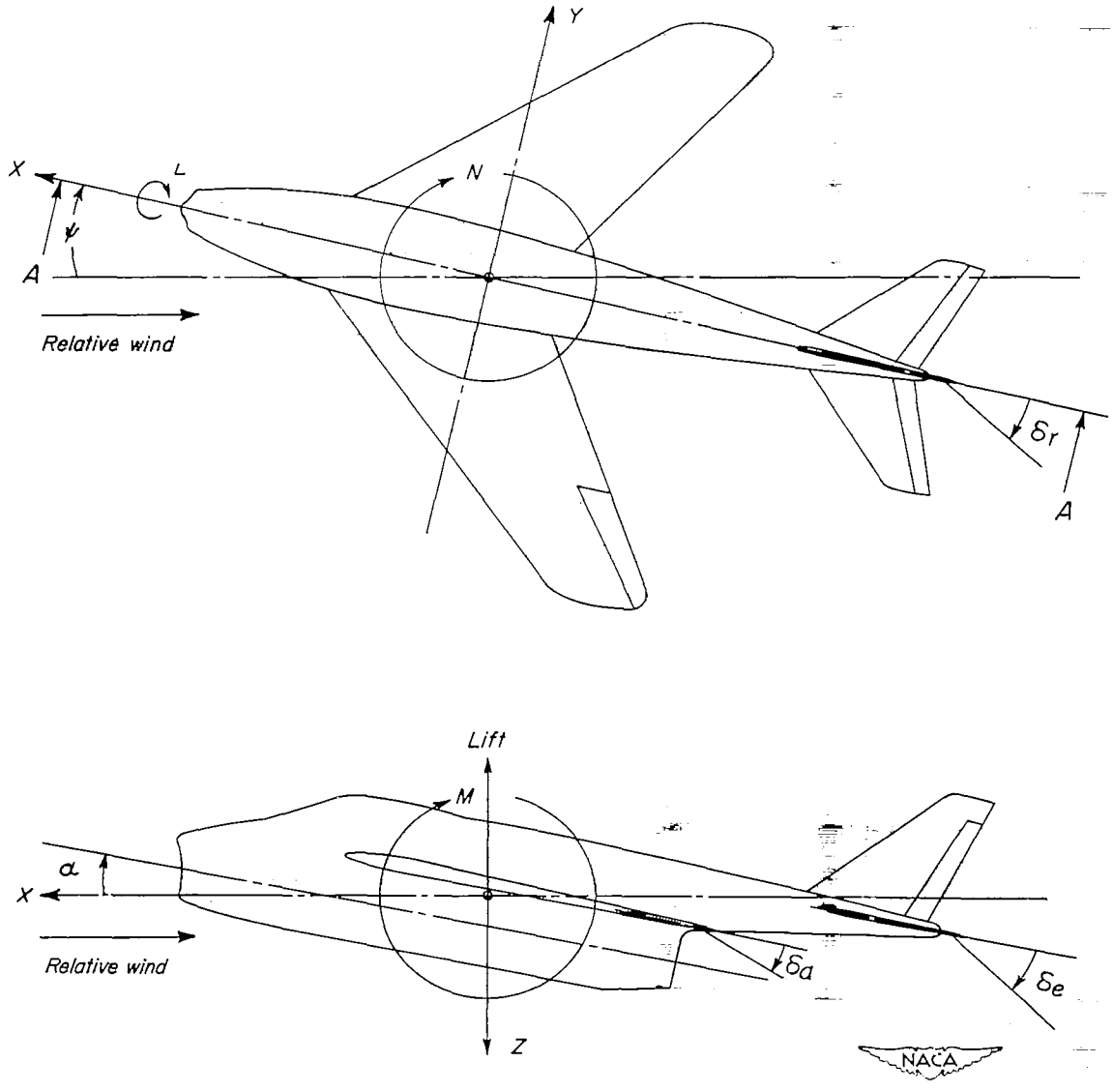

View A-A

Figure 1.- System of axes and control-surface deflections. Positive values of forces, moments, and angles are indicated by arrows.

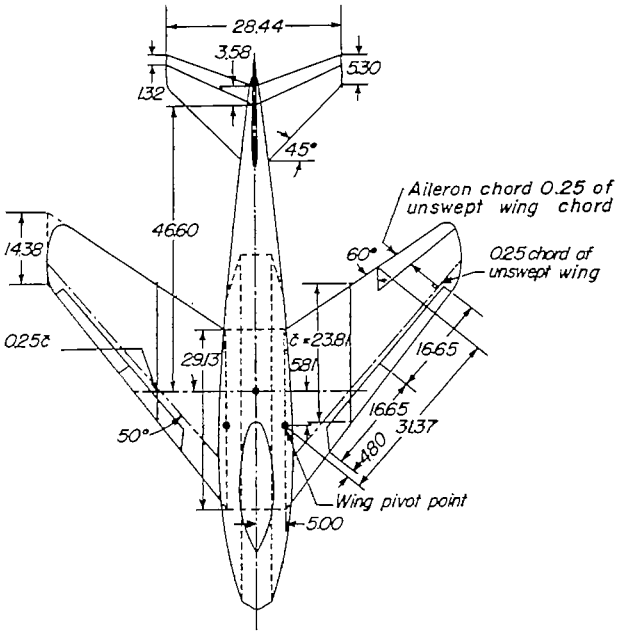

PHYSICAL CHARACTERISTICS

Wing:				
Sweep, deg	20	35	50	60
Area, sq ft	10.33	10.45	10.80	11.33
Aspect ratio	5.76	4.56	2.98	1.92
Span, ft	7.72	6.90	5.67	4.66
Mean aerodynamic chord, ft	1.396	1.579	1.985	2.535
Incidence, deg				0
Dihedral, deg				-2
Airfoil section perpendicular to 0.25c:				
Root				NACA $64_{(10)}$-010.3
Tip				NACA 64-008
Horizontal tail:				
Area, sq ft				1.94
Aspect ratio				2.89
Vertical tail:				
Area, sq ft				1.33
Aspect ratio				1.46

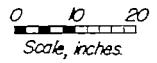

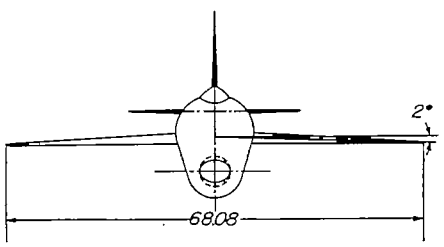

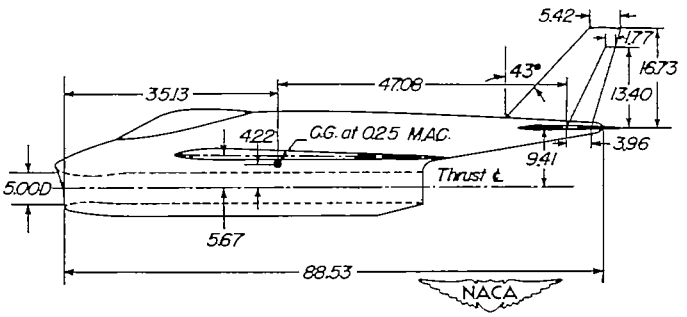

Figure 2.- General arrangement of test model.

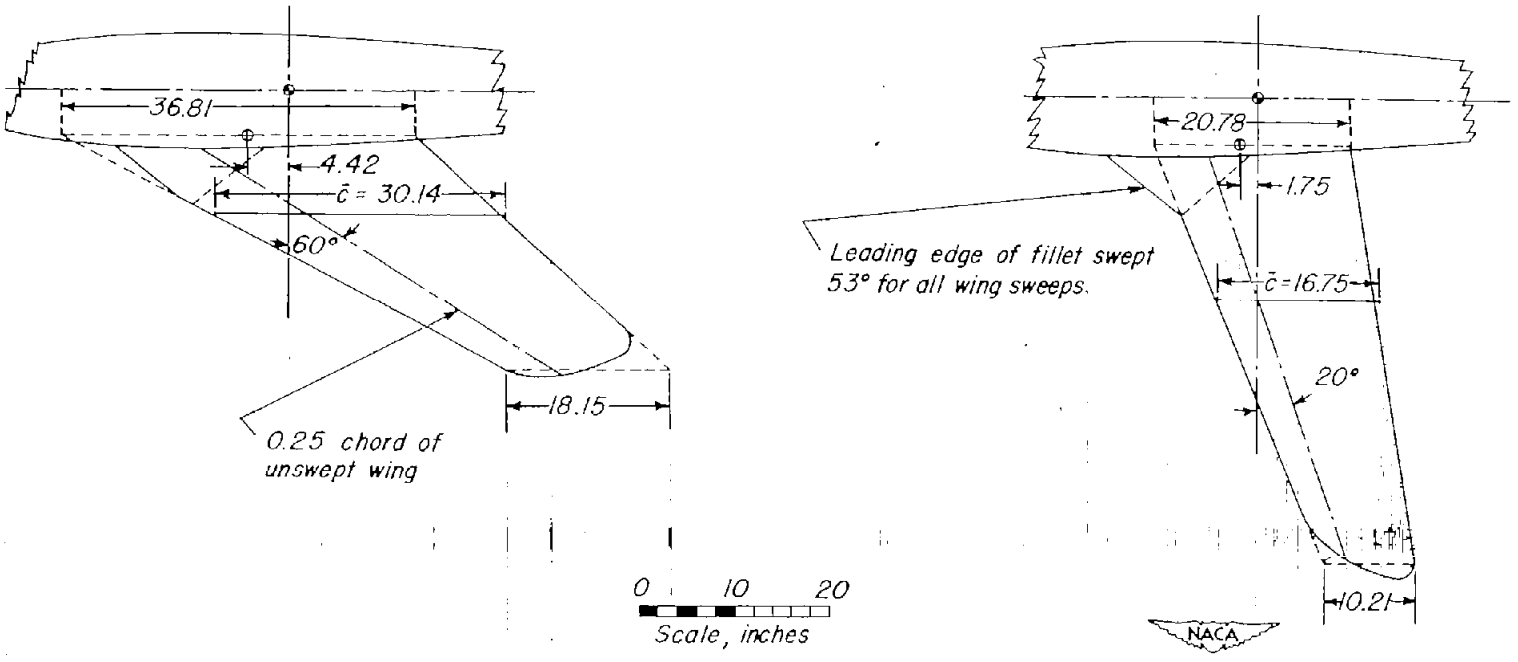

Figure 2.- Concluded.

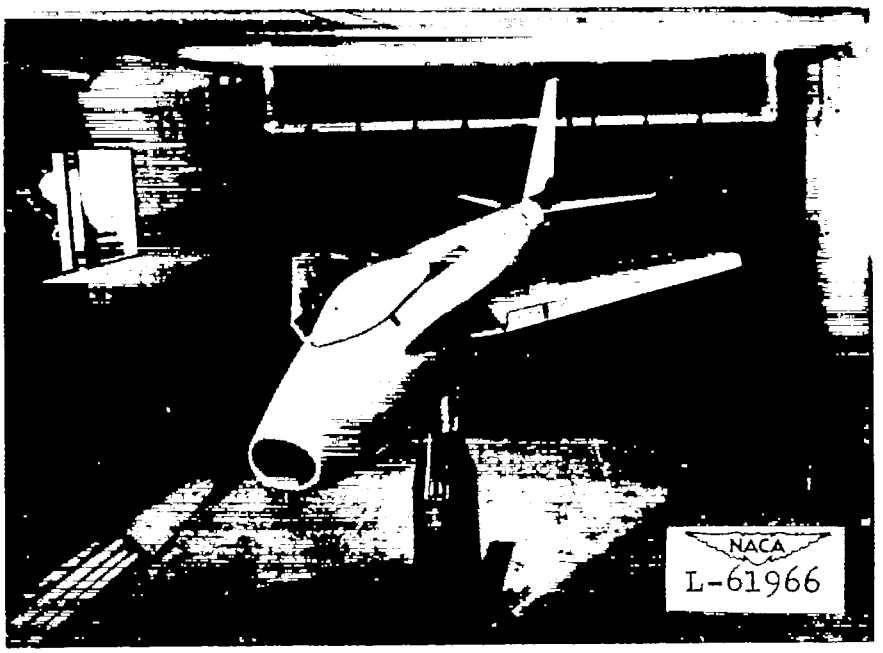

Figure 3.- View of test model as mounted in tunnel.

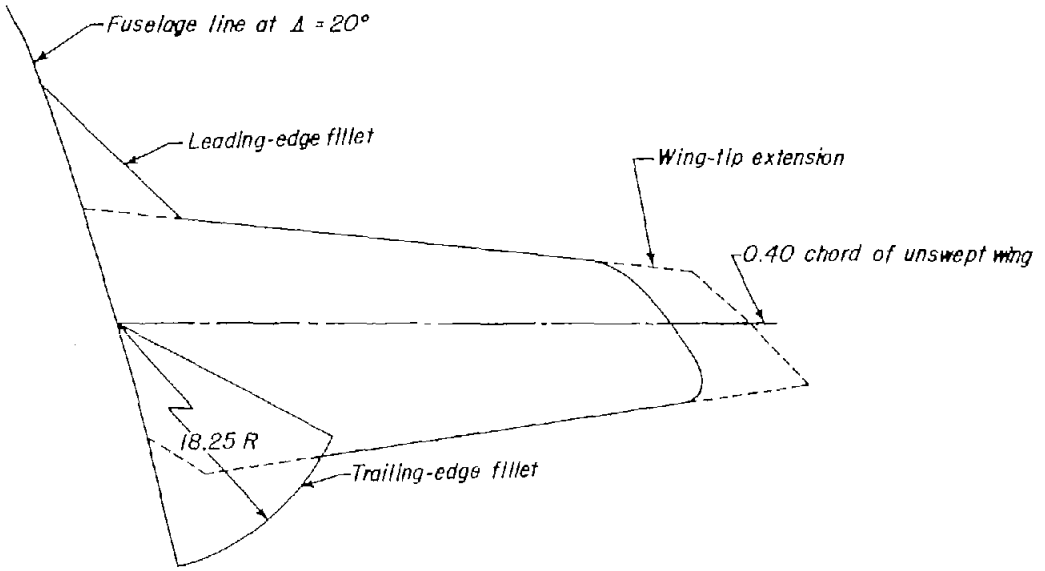

PHYSICAL CHARACTERISTICS OF WING

WITH TIP EXTENSION

Sweep, deg	60
Area, sq ft	11.96
Aspect ratio	2.25
Span, ft	5.19
Mean aerodynamic chord, ft	2.45

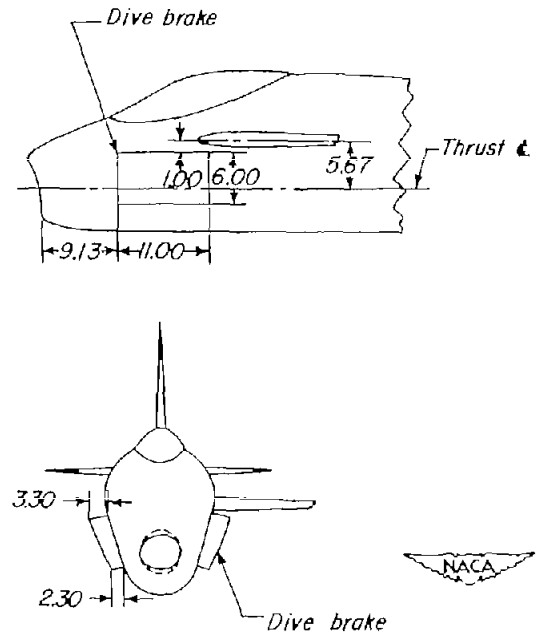

Figure 4.- Details of wing-tip extension, trailing-edge fillet, and dive brakes.

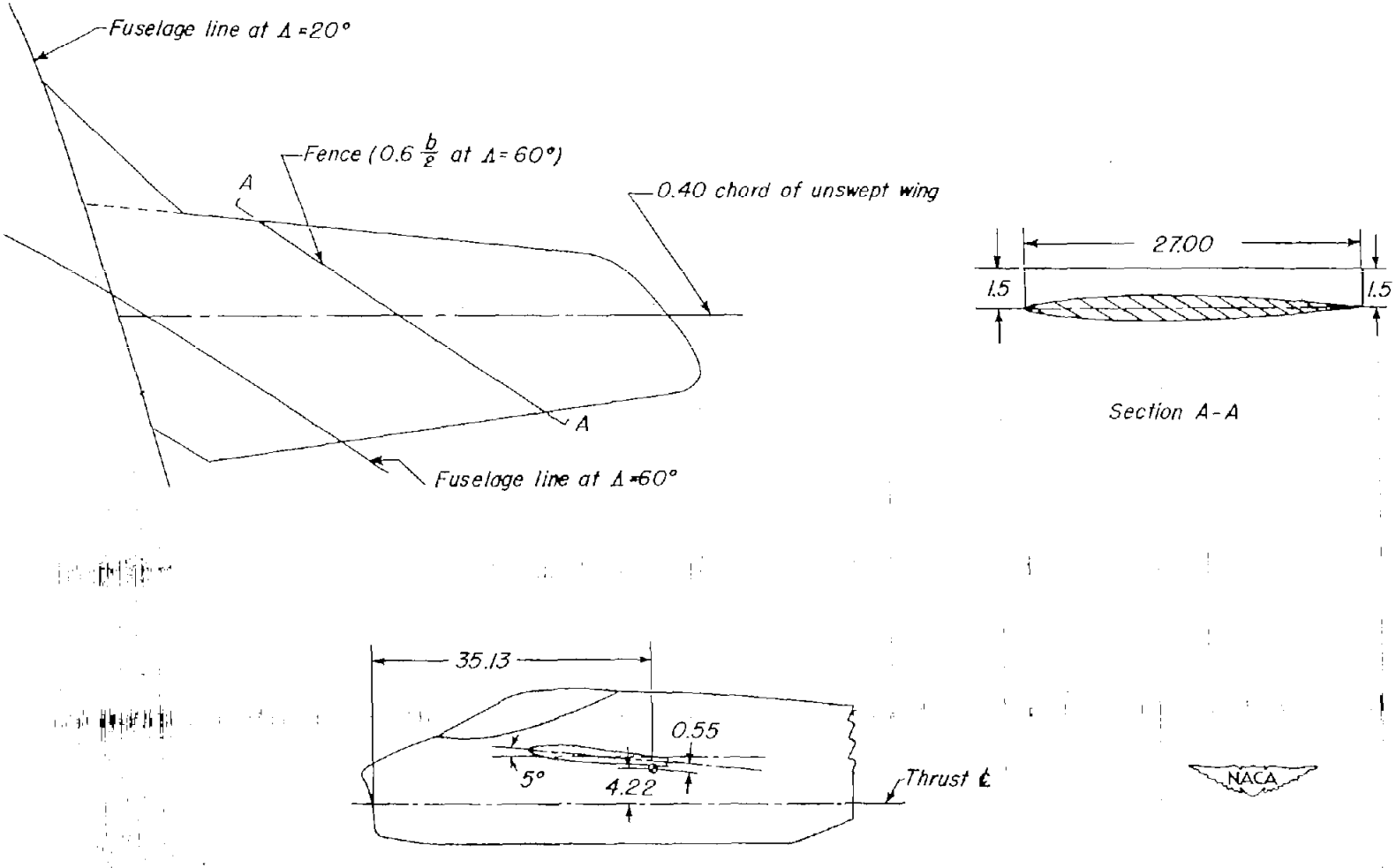

Figure 5.- Details of wing fence and 5° wing incidence.

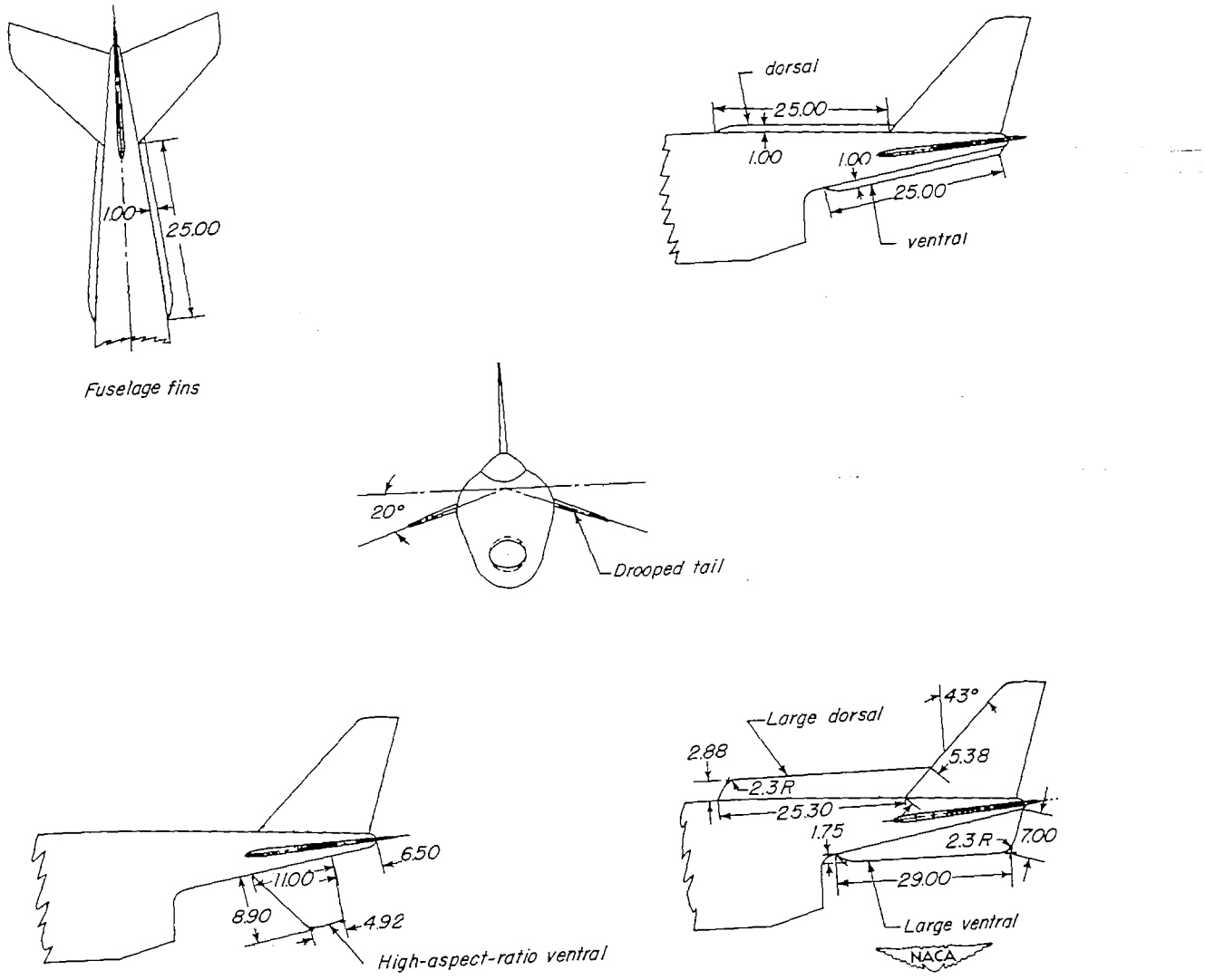

Figure 6.- Details of fins and drooped horizontal tail.

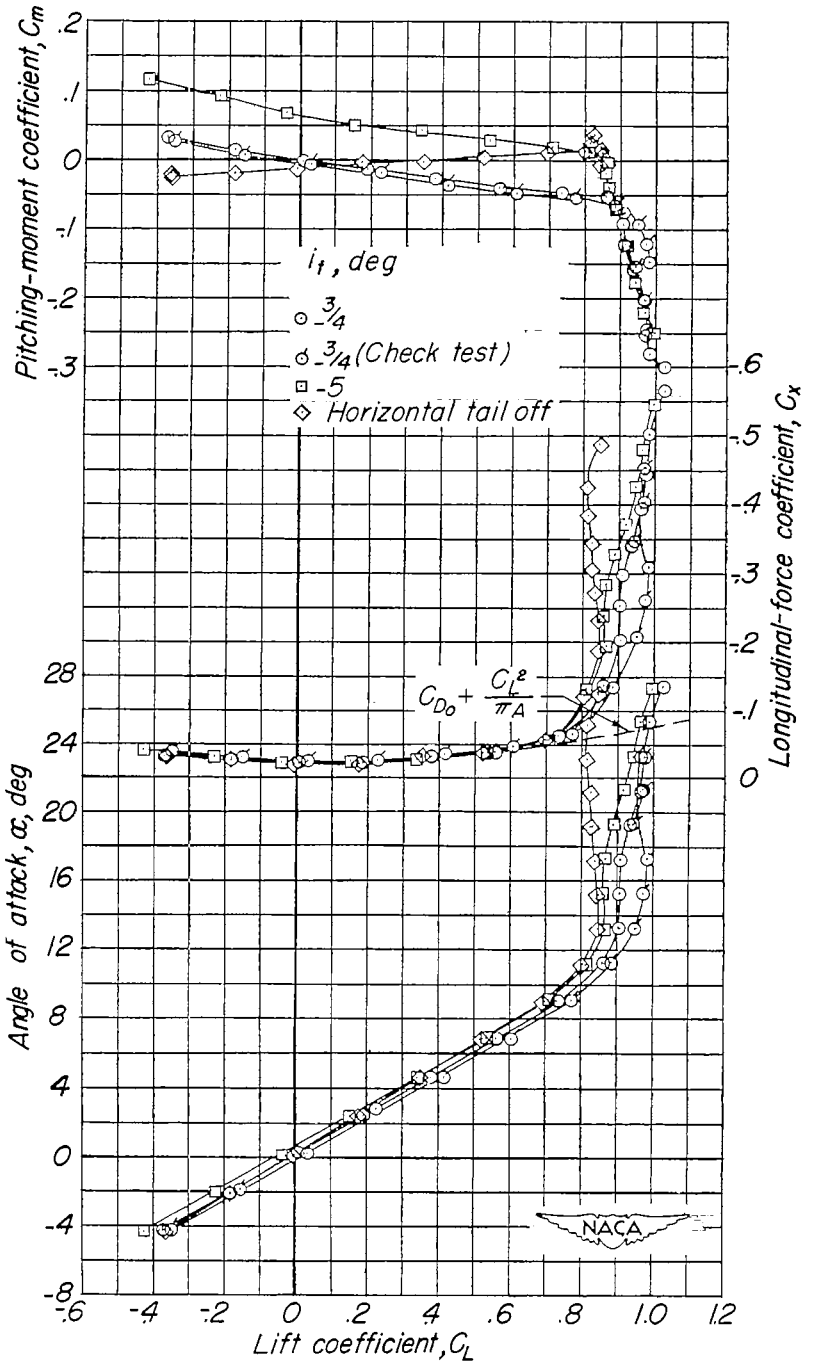

(a) $\Lambda = 20^\circ$.

Figure 7.- The effect of tail incidence on the aerodynamic characteristics of the test model.

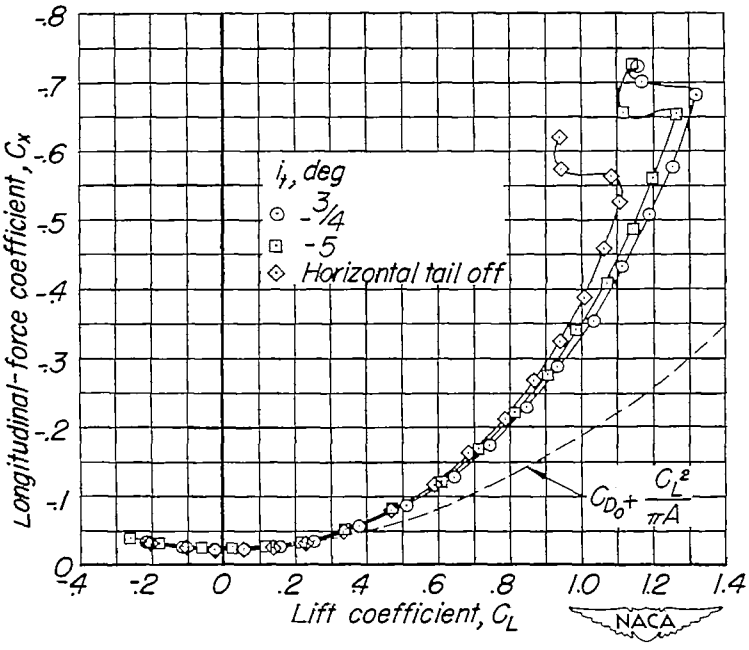

(b) Concluded.

Figure 7.- Concluded.

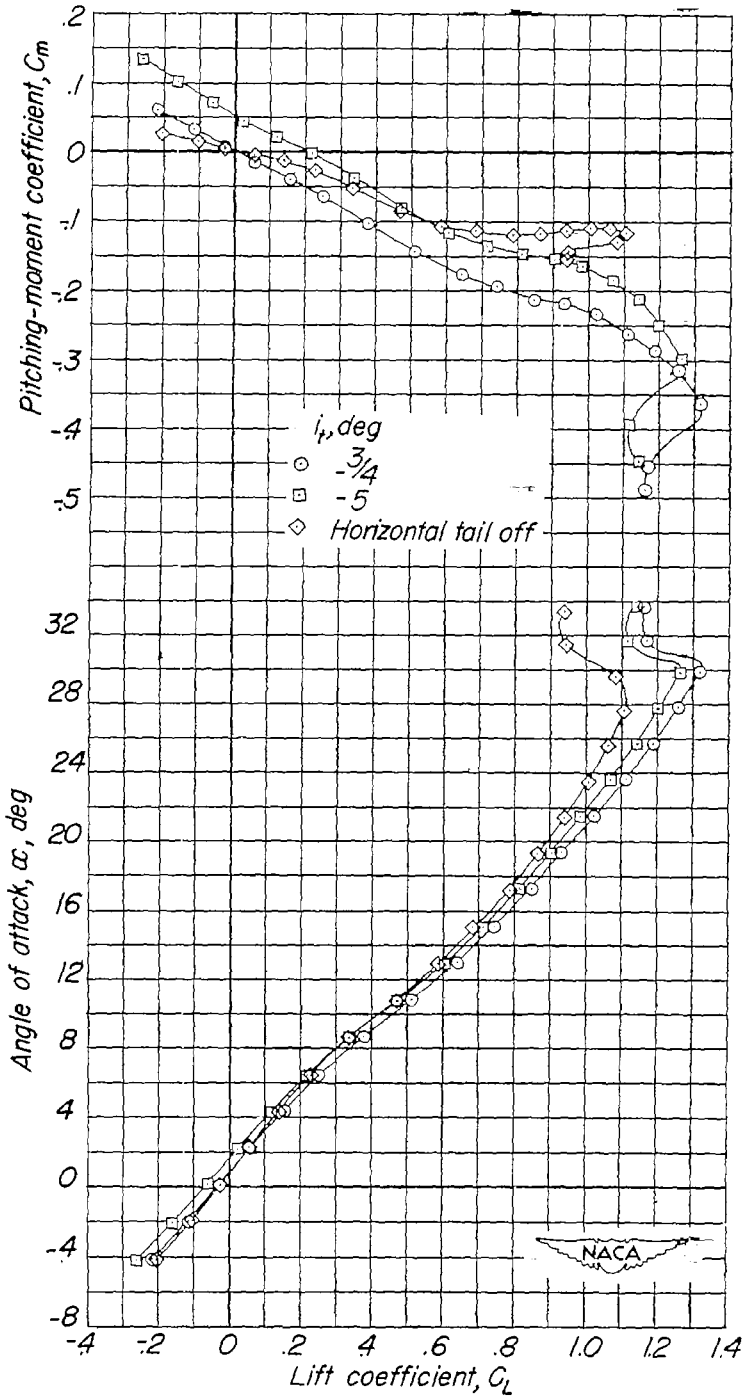

(b) $\Lambda = 60^\circ$.

Figure 7.- Continued.

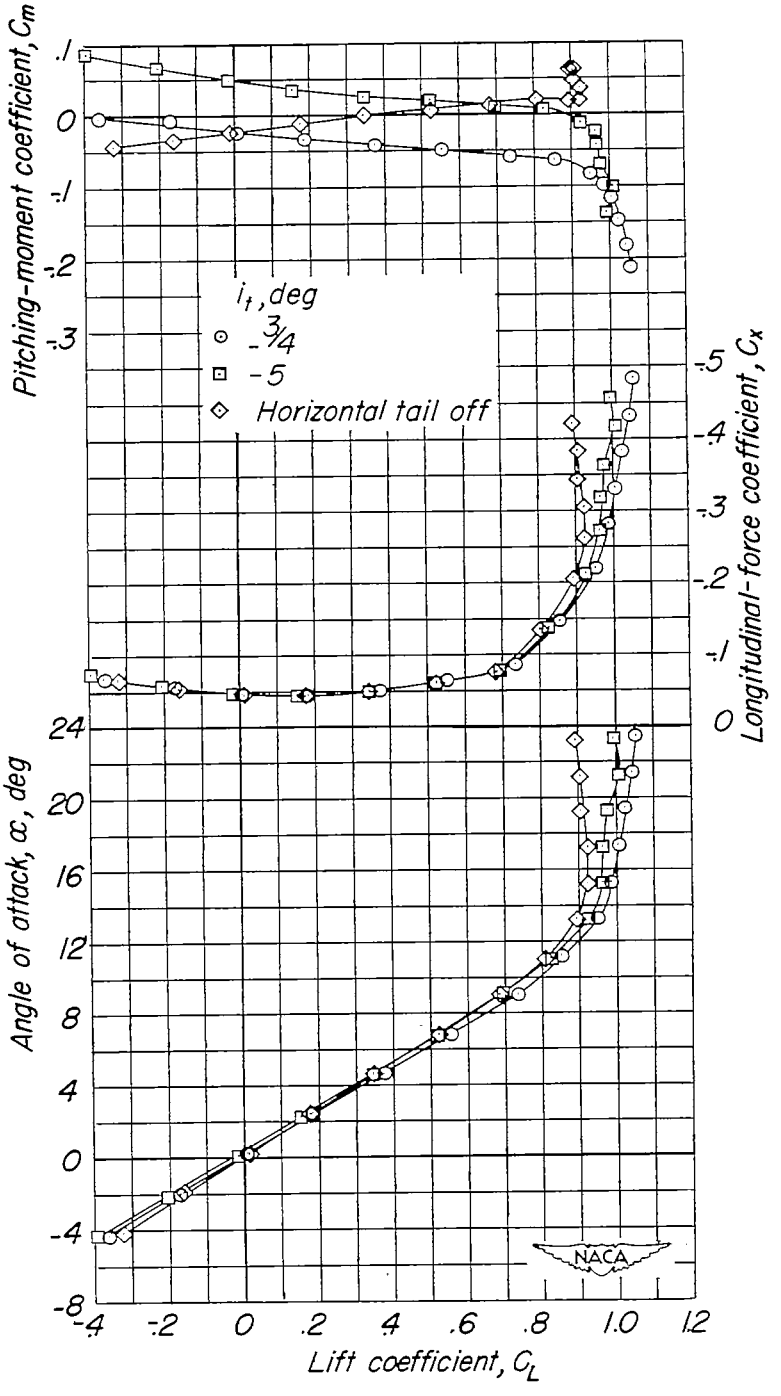

(a) $\Lambda = 20^\circ$.

Figure 8.- The effect of tail incidence on the aerodynamic characteristics of the test model. Dive brakes extended.

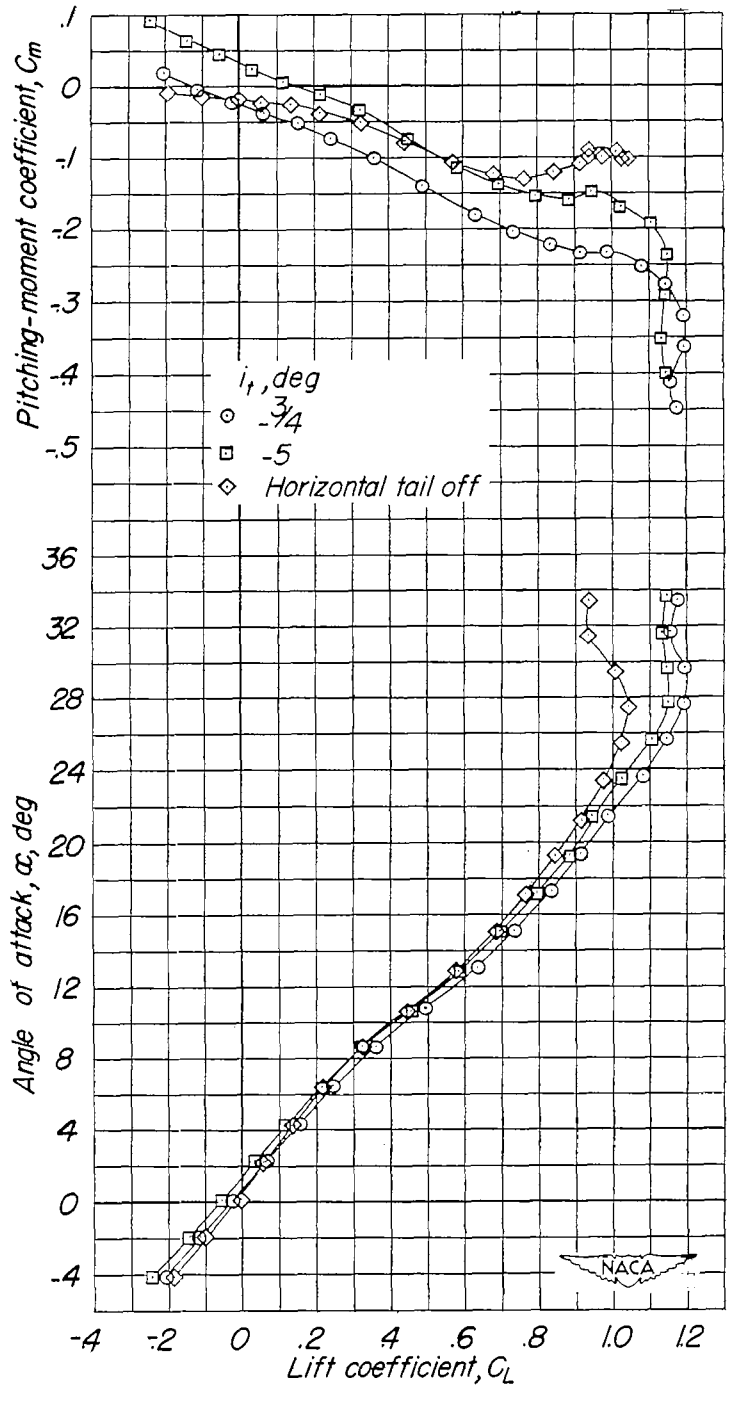

(b) $\Lambda = 60^\circ$.

Figure 8.- Continued.

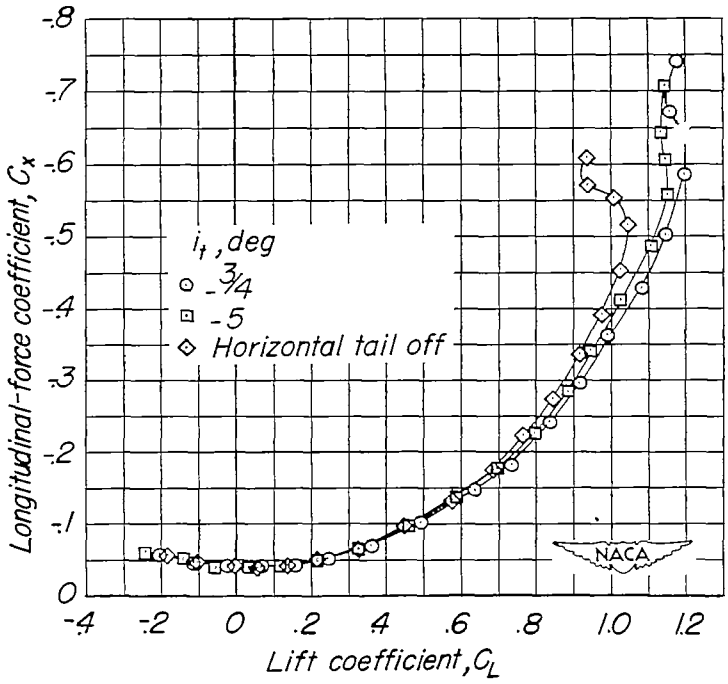

(b) Concluded.

Figure 8.- Concluded.

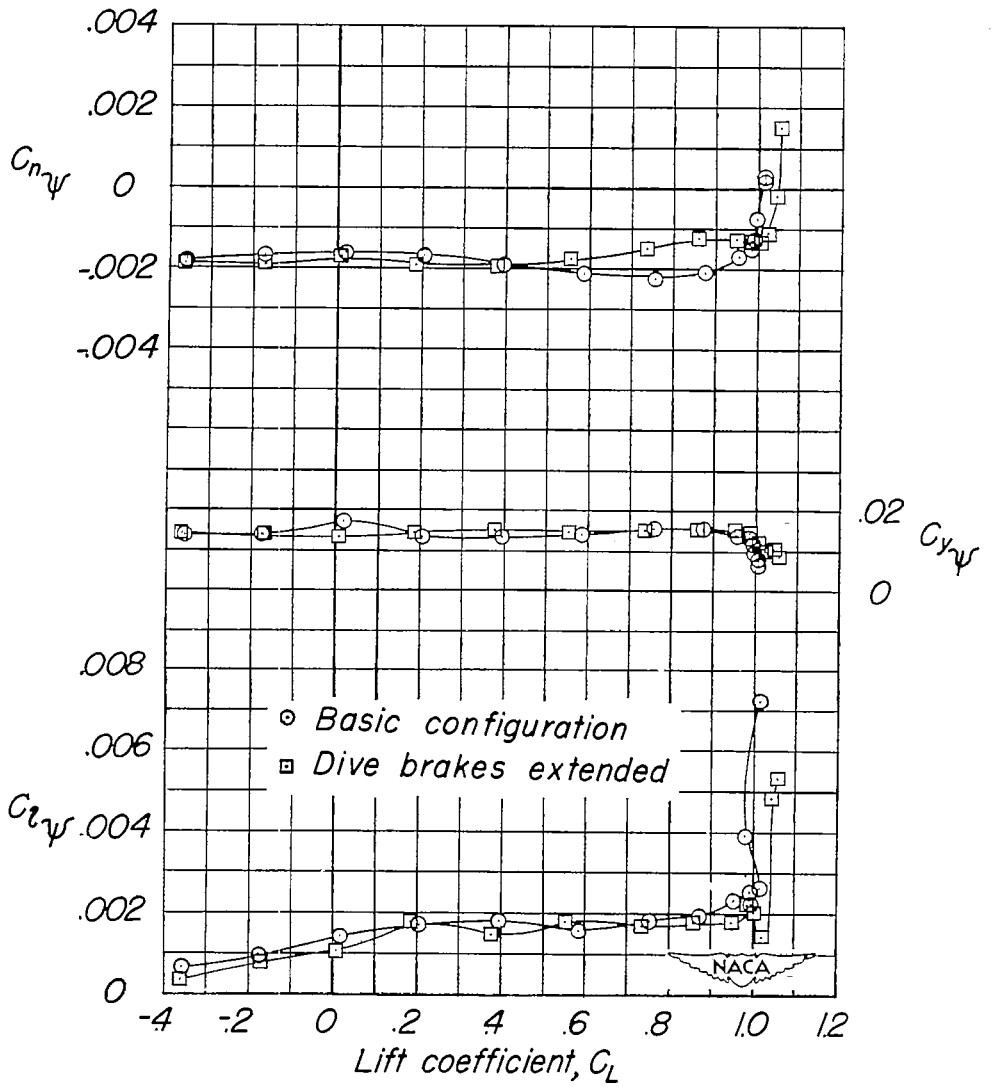

(a) $\Lambda = 20^\circ$.

Figure 9.- The effect of dive brakes on the lateral-stability parameters of the test model. $i_t = -\frac{3^\circ}{4}$.

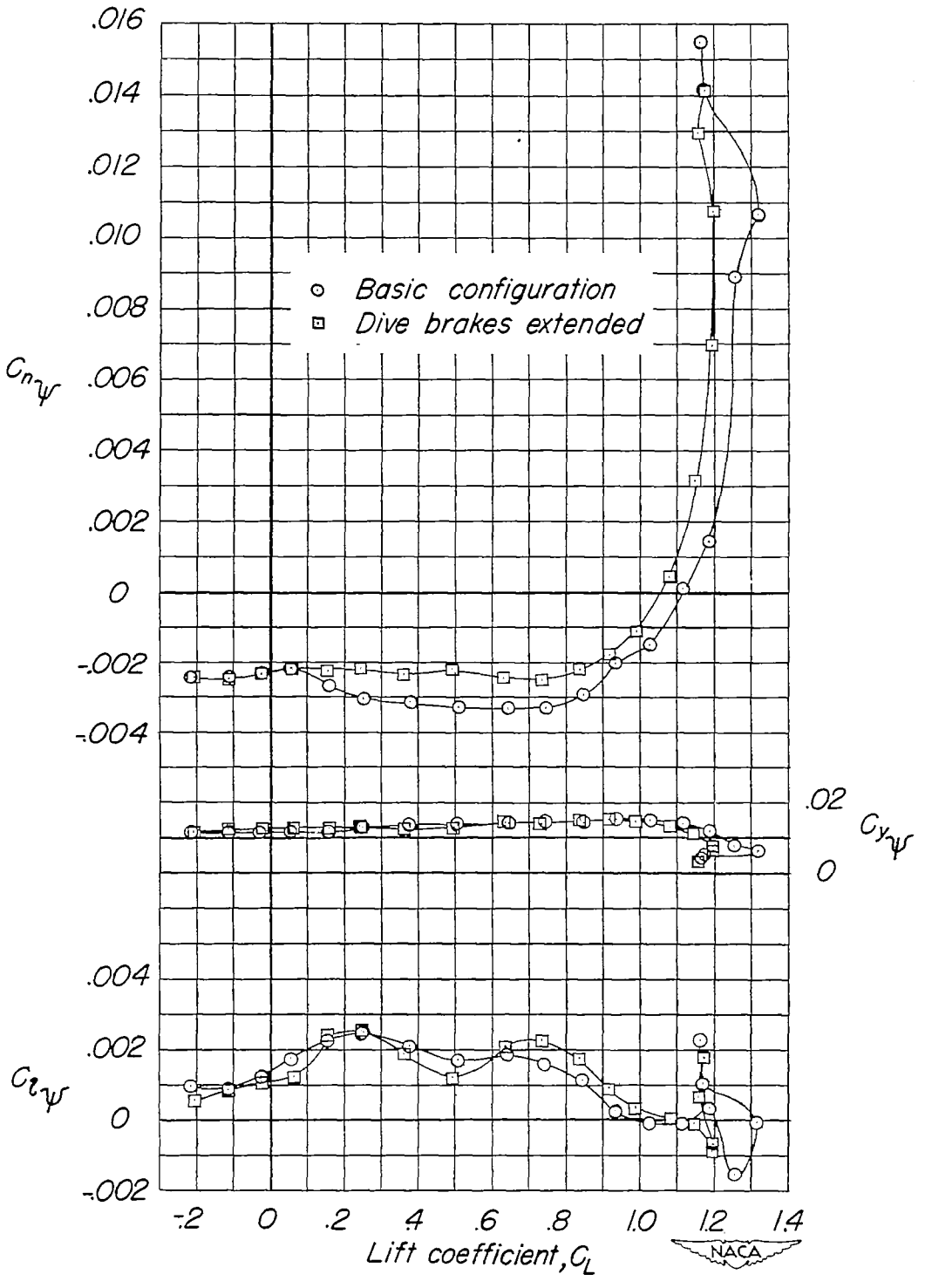

(b) $\Lambda = 60^\circ$.

Figure 9.- Concluded.

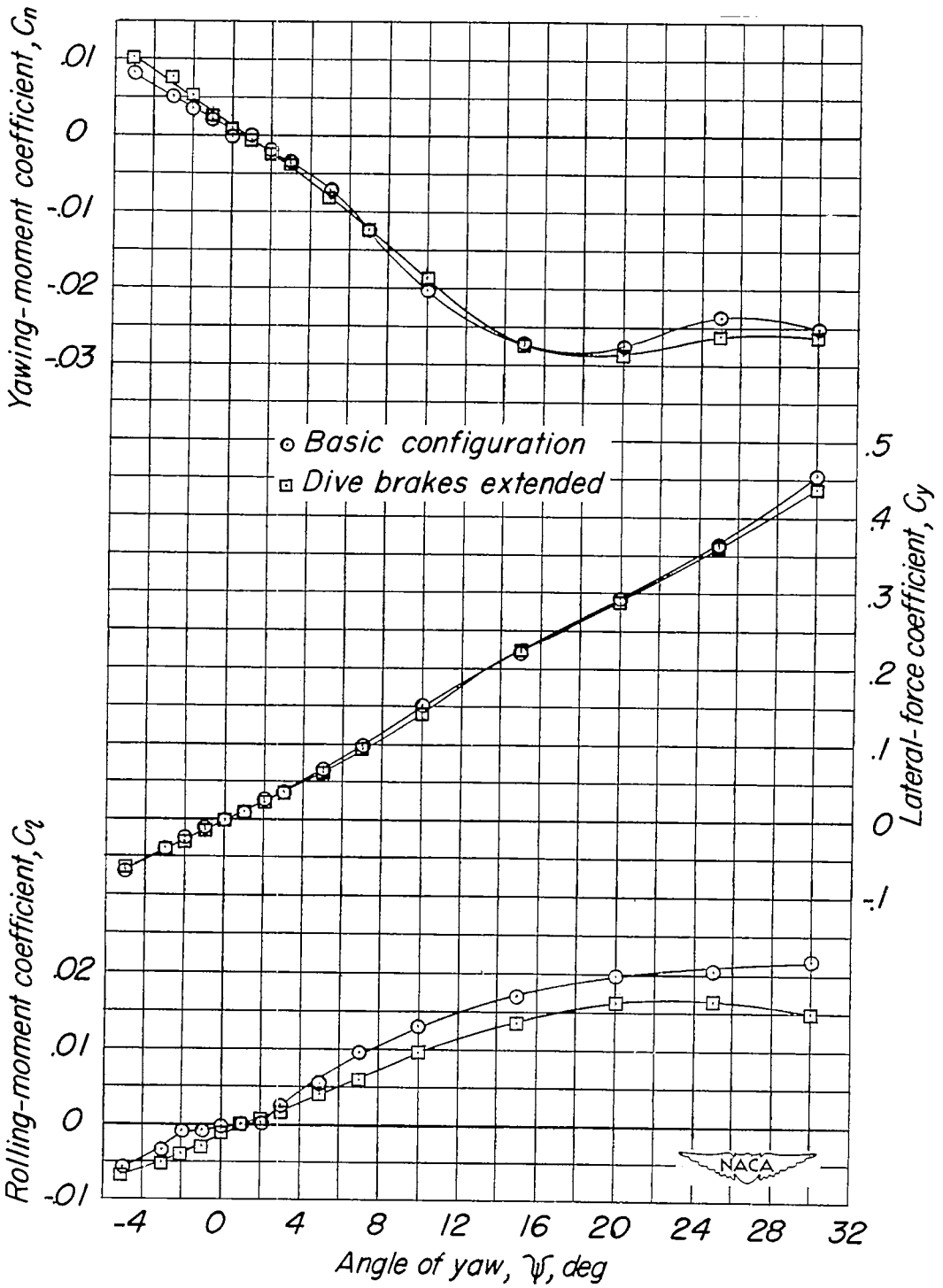

Figure 10.- The effect of dive brakes on the aerodynamic characteristics in yaw of the test model. $\Lambda = 20^\circ$, $i_t = -\frac{3}{4}^\circ$, $\alpha = 0.22^\circ$.

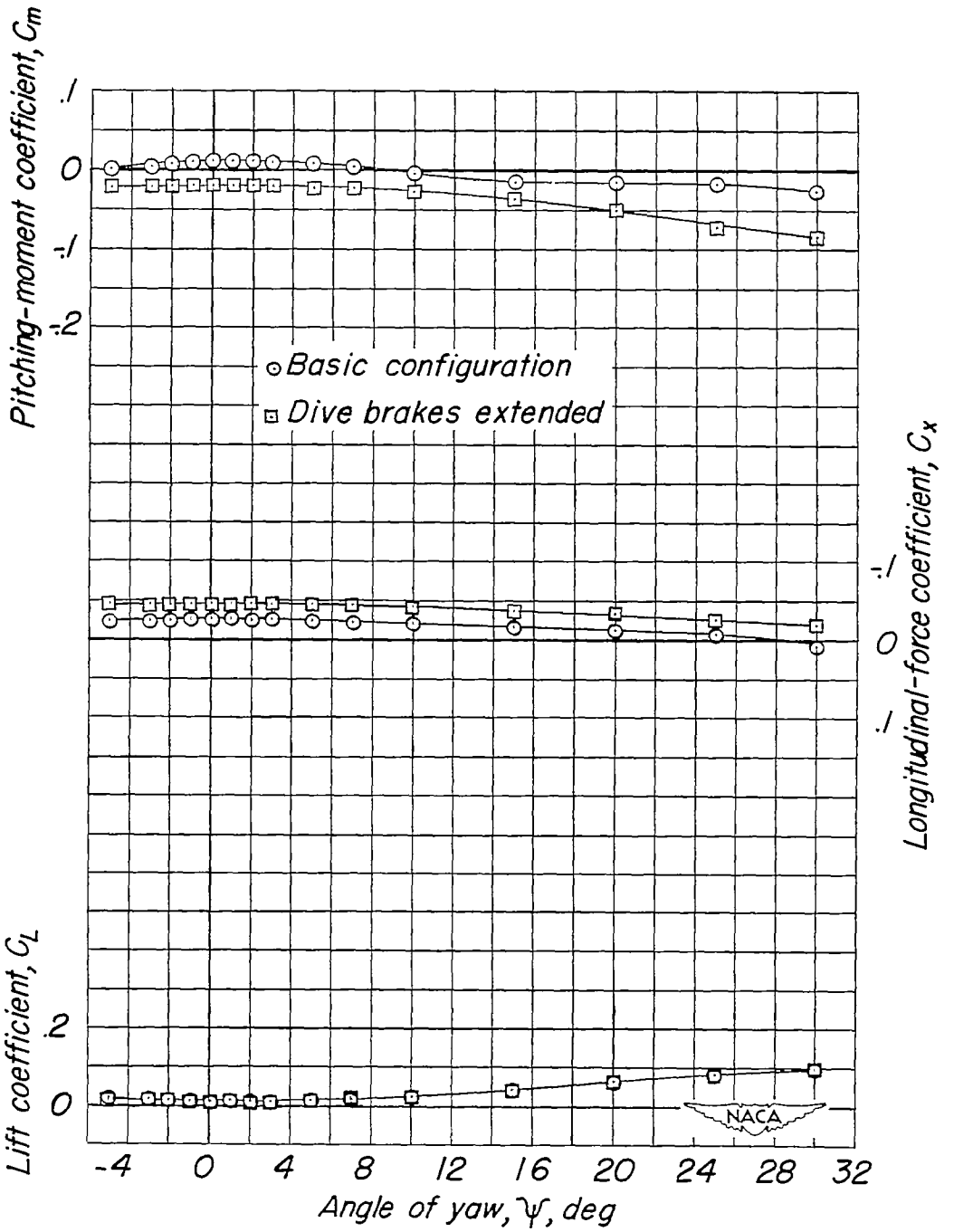

Figure 10.- Concluded.

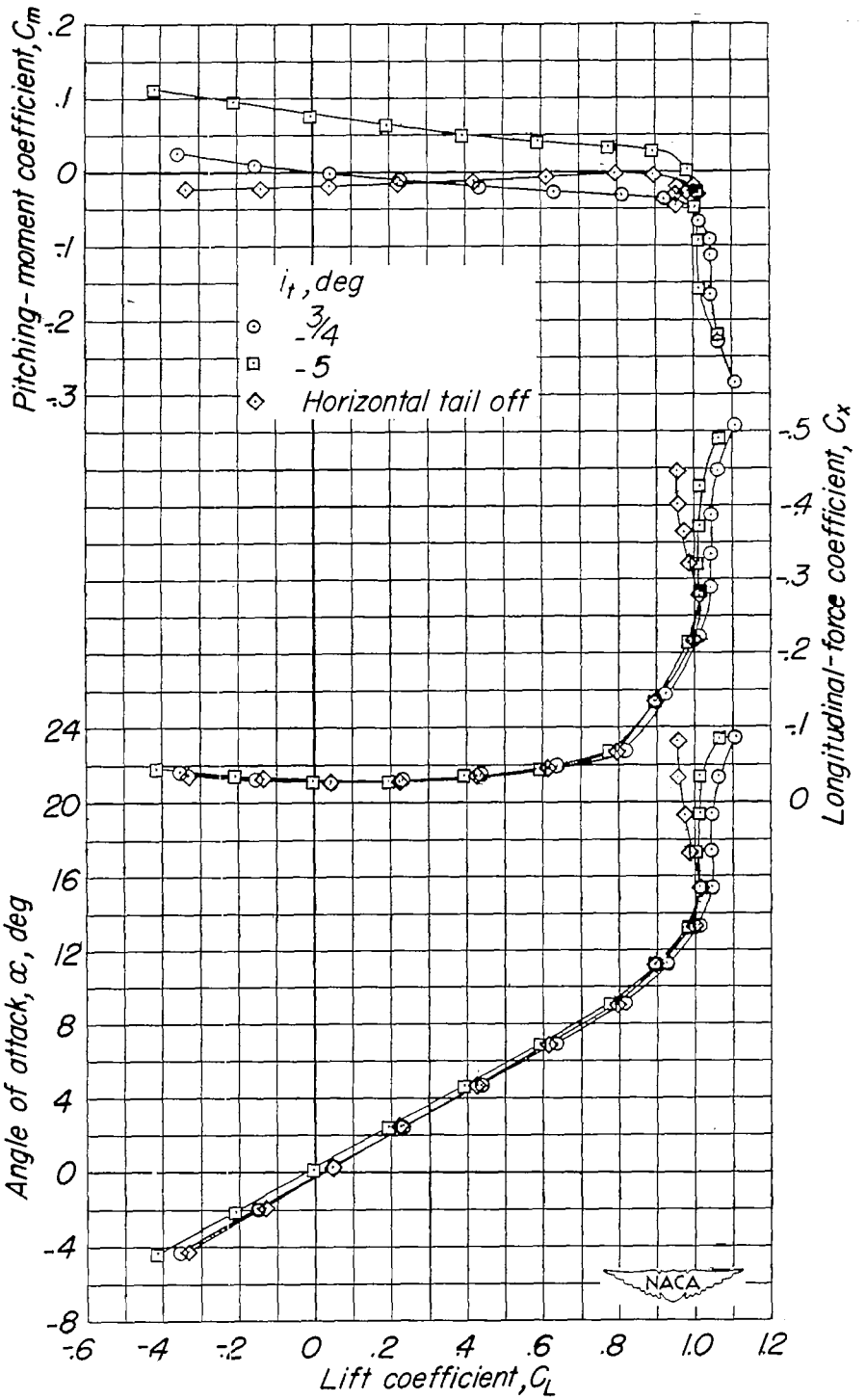

Figure 11.- The effect of tail incidence on the aerodynamic characteristics of the test model. Trailing-edge fillets, $\Lambda = 20^\circ$.

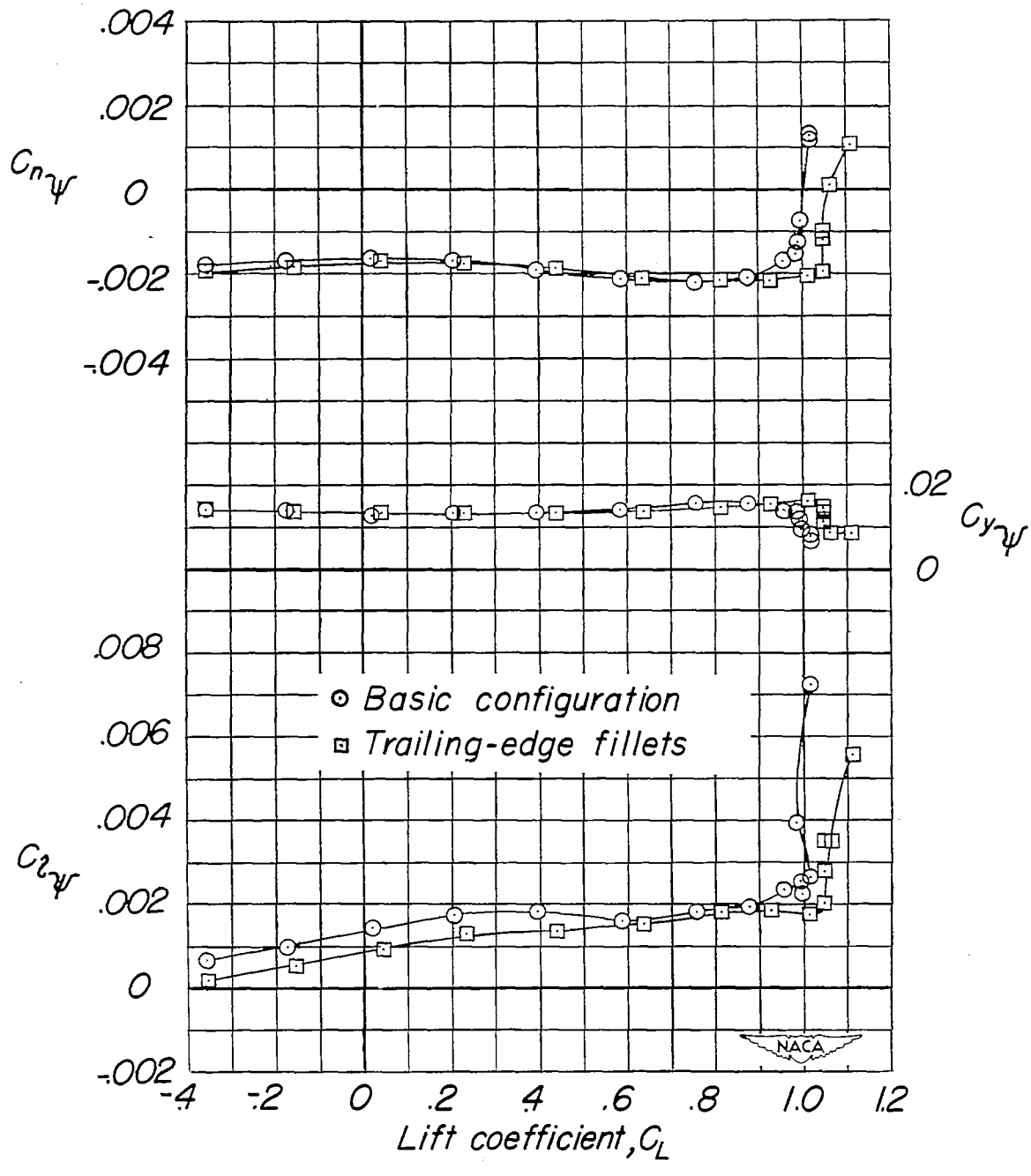

Figure 12.- The effect of trailing-edge fillets on the lateral-stability parameters of the test model. $\Lambda = 20^\circ$, $i_t = -\frac{3}{4}^\circ$.

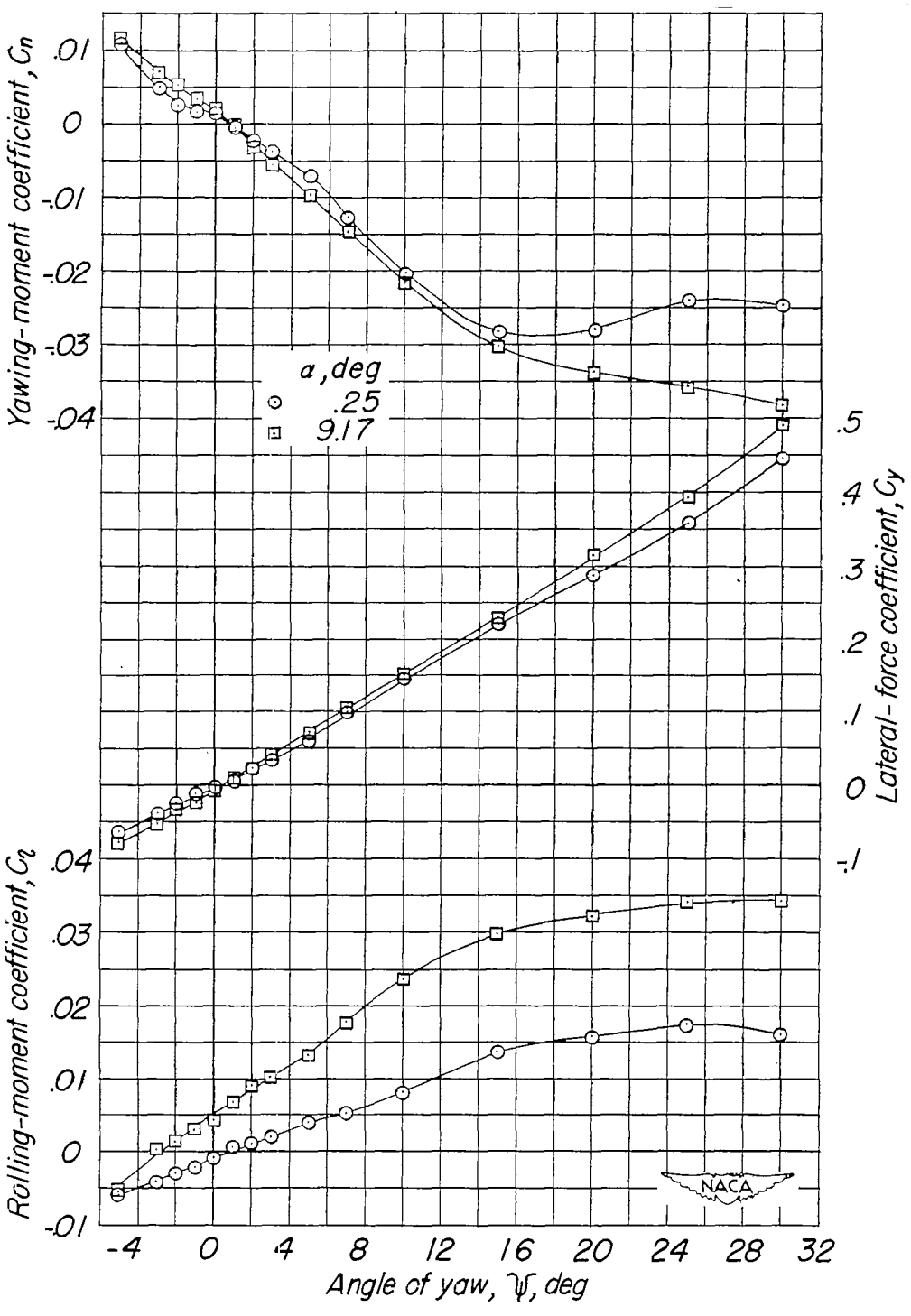

Figure 13.- The effect of angle of attack on the aerodynamic characteristics in yaw of the test model. Trailing-edge fillets, $\Lambda = 20^\circ$, $i_t = -\frac{3}{4}^\circ$.

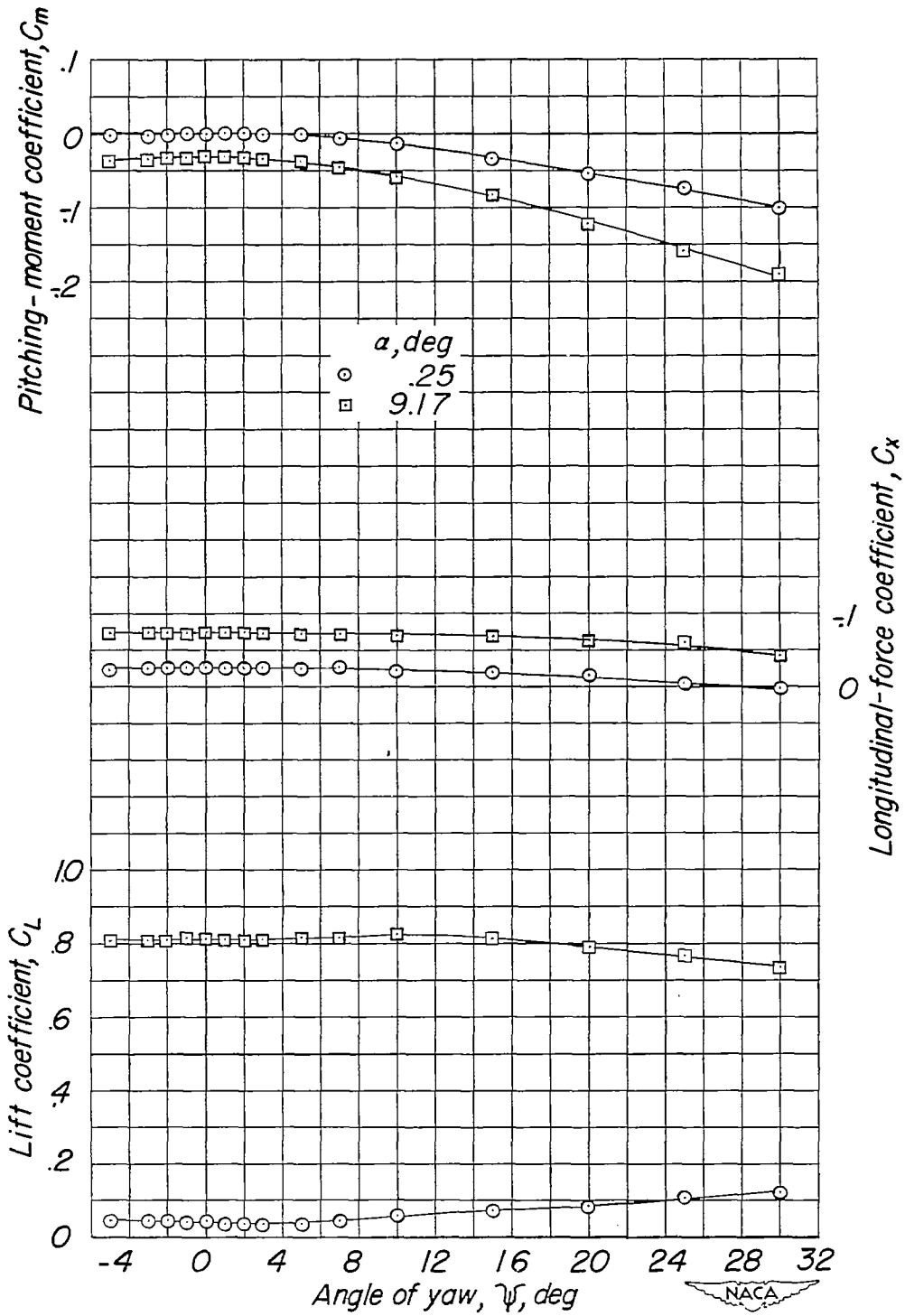

Figure 13.- Concluded.

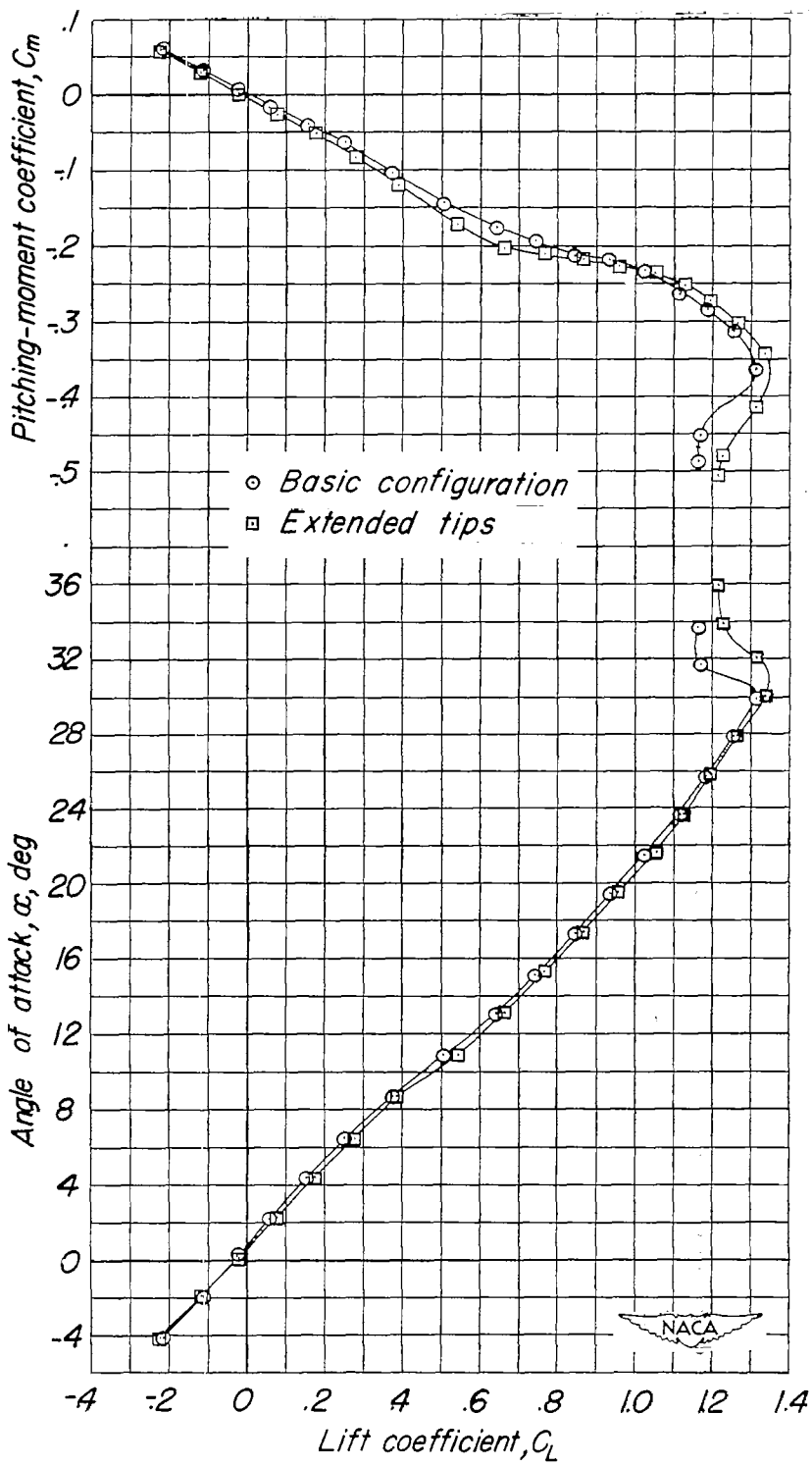

Figure 14.- The effect of extended wing tips on the aerodynamic characteristics of the test model. $\Lambda = 60^\circ$, $i_t = -\frac{3^\circ}{4}$.

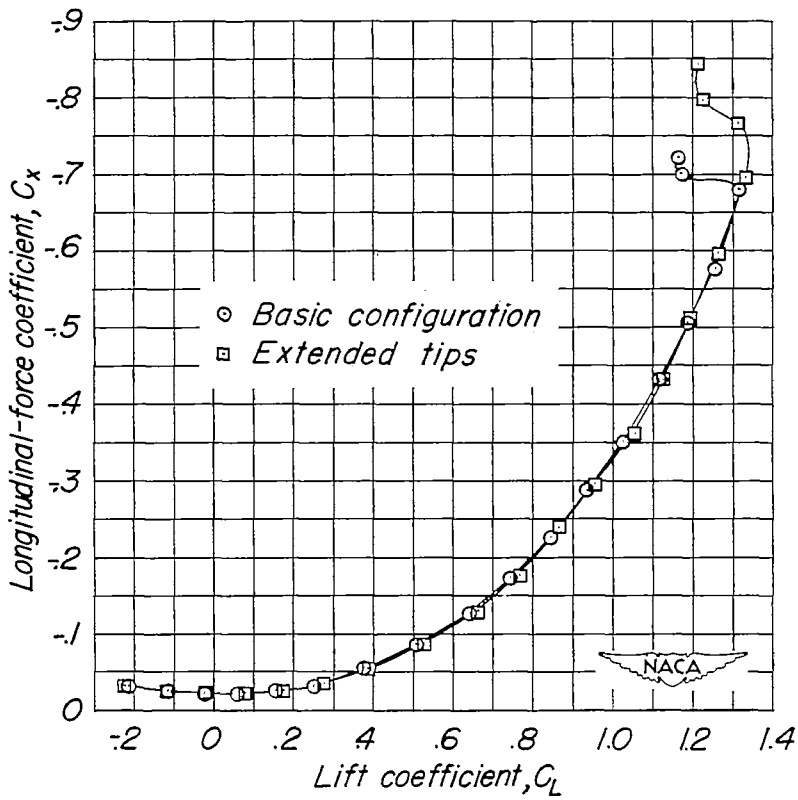

Figure 14.- Concluded.

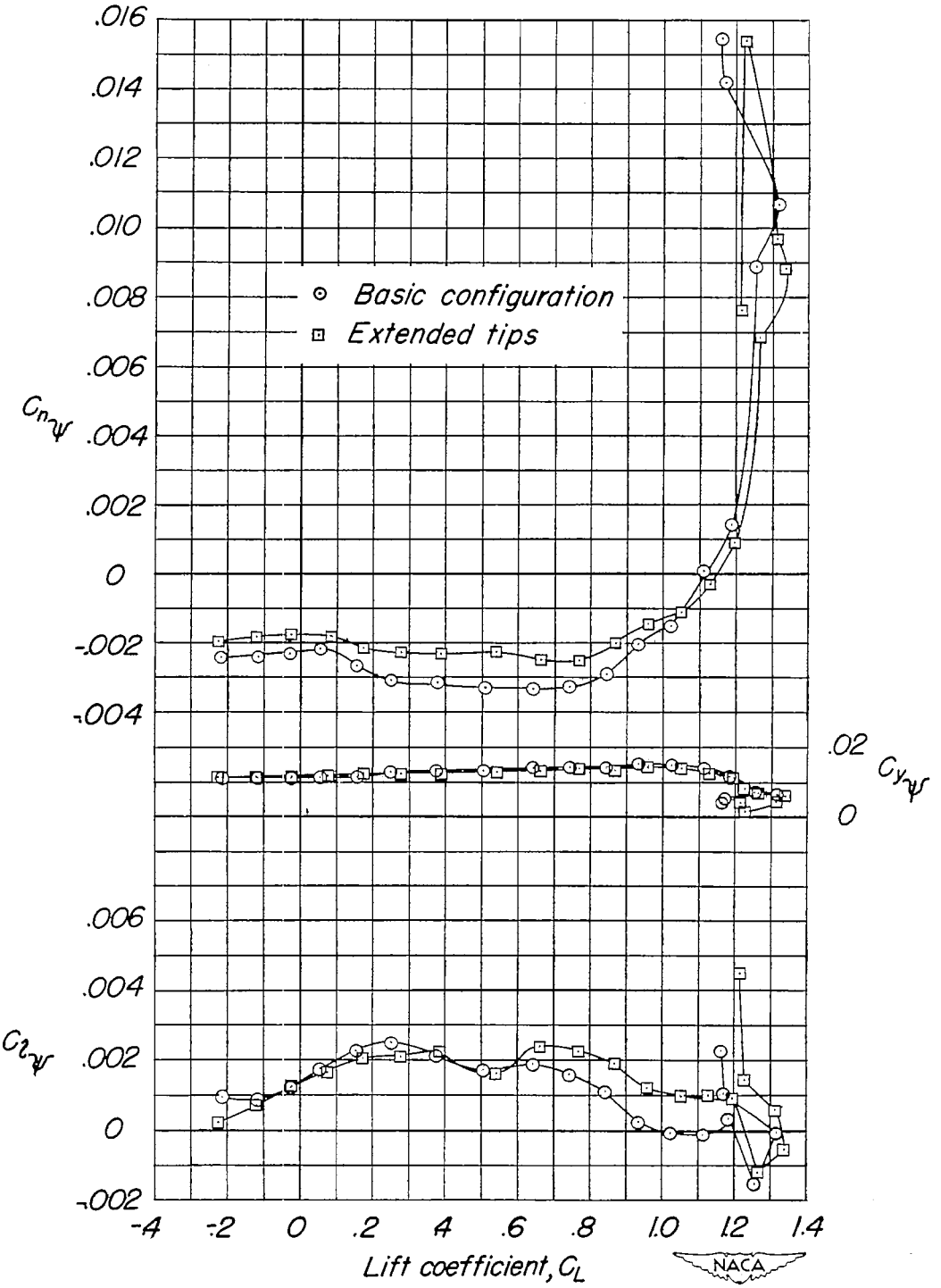

Figure 15.- The effect of extended wing tips on the lateral-stability parameters of the test model. $\Lambda = 60^\circ$, $i_t = -\frac{3}{4}^\circ$.

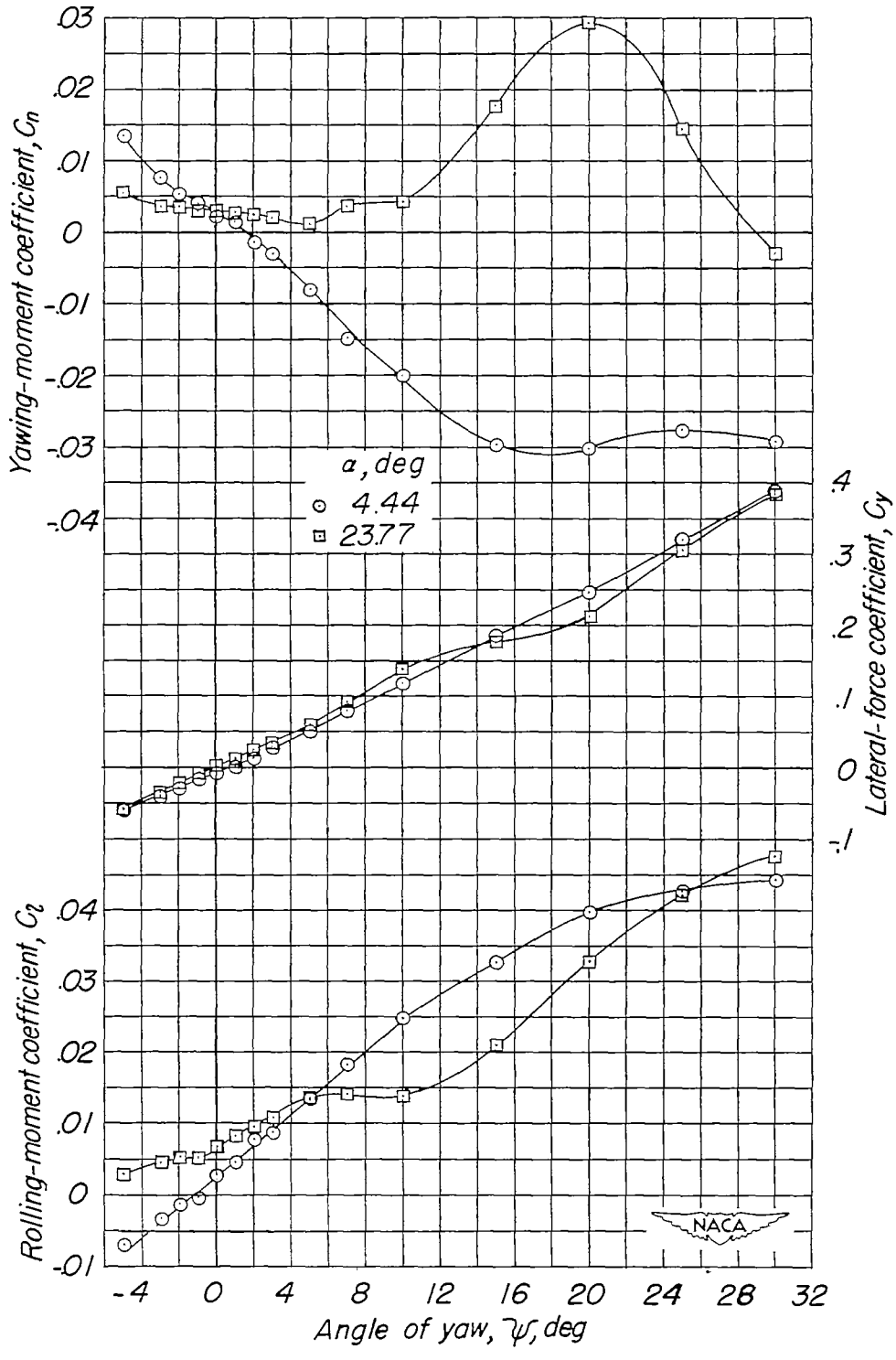

Figure 16.- The effect of angle of attack on the aerodynamic characteristics in yaw of the test model. Extended wing tips, $\Lambda = 60^\circ$, $i_t = -\frac{3}{4}^\circ$.

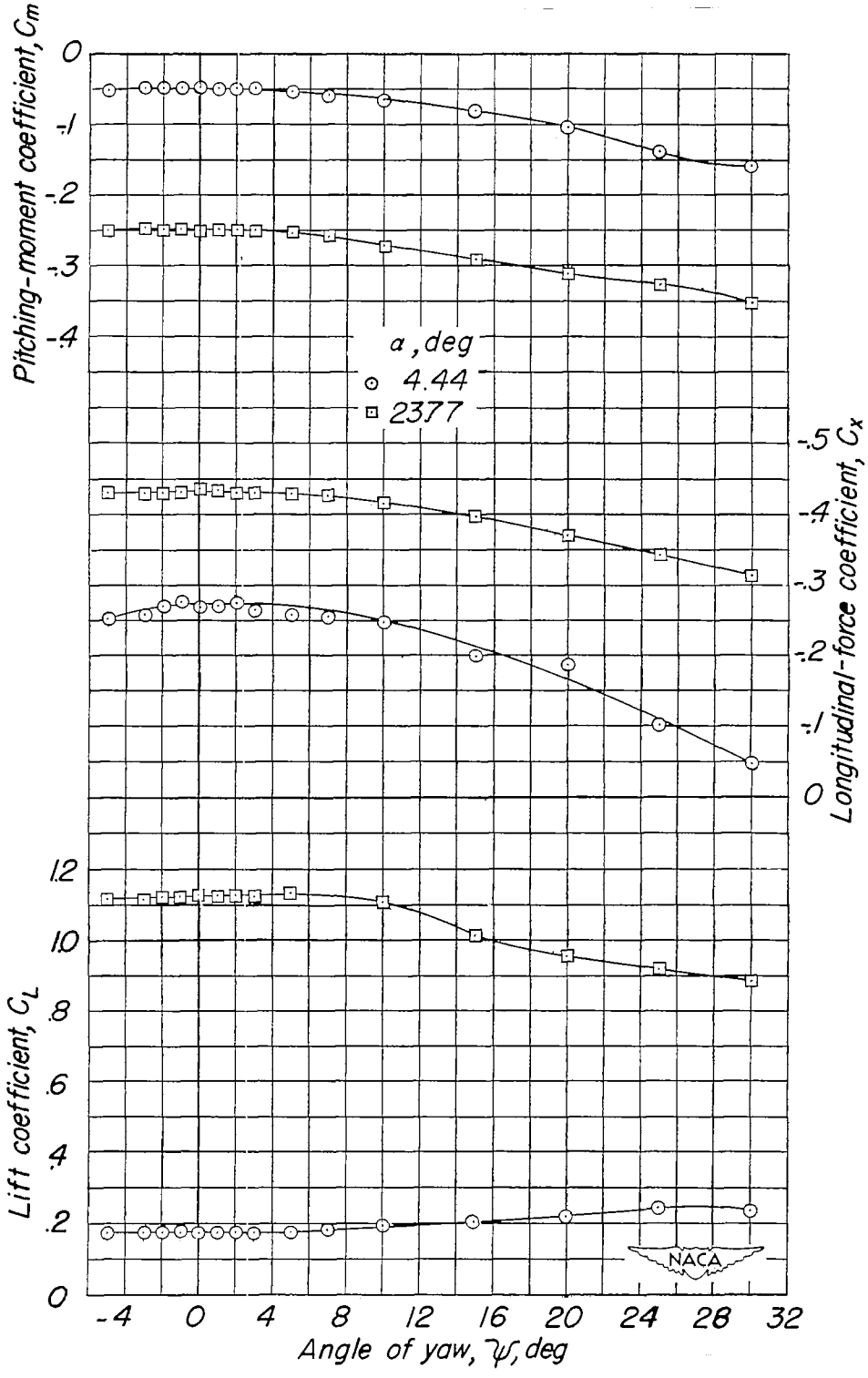

Figure 16.- Concluded.

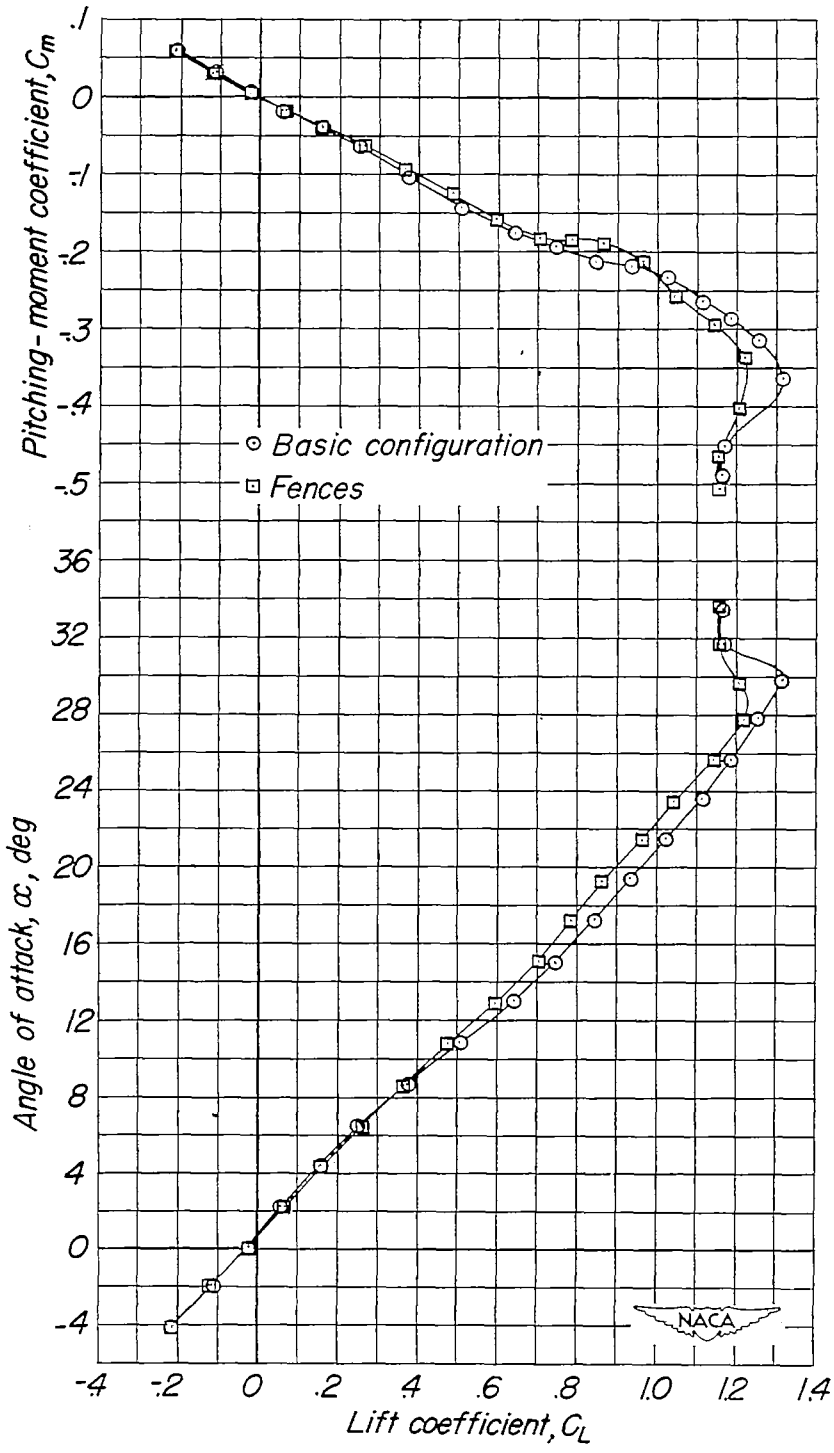

Figure 17.- The effect of fences on the aerodynamic characteristics of the test model. $\Lambda = 60^\circ$, $i_t = -\frac{3}{4}^\circ$.

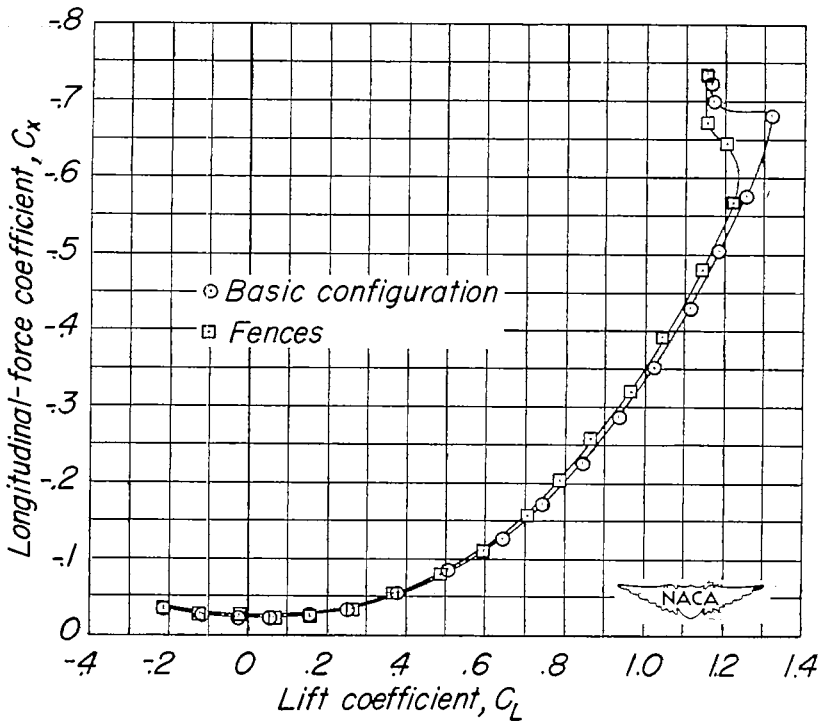

Figure 17.- Concluded.

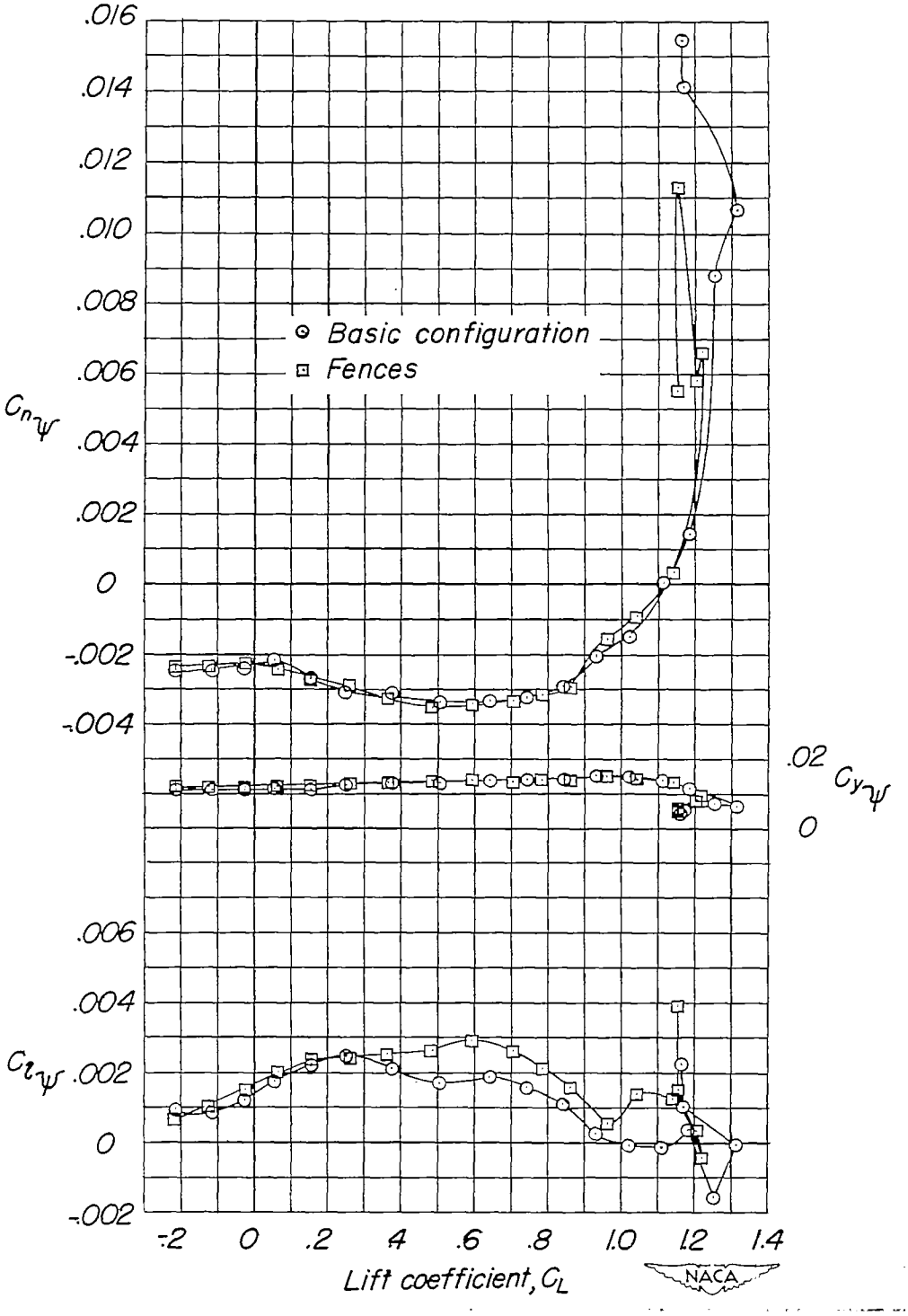

Figure 18.- The effect of fences on the lateral-stability characteristics of the test model. $\Lambda = 60^\circ$, $i_t = -\frac{3}{4}^\circ$.

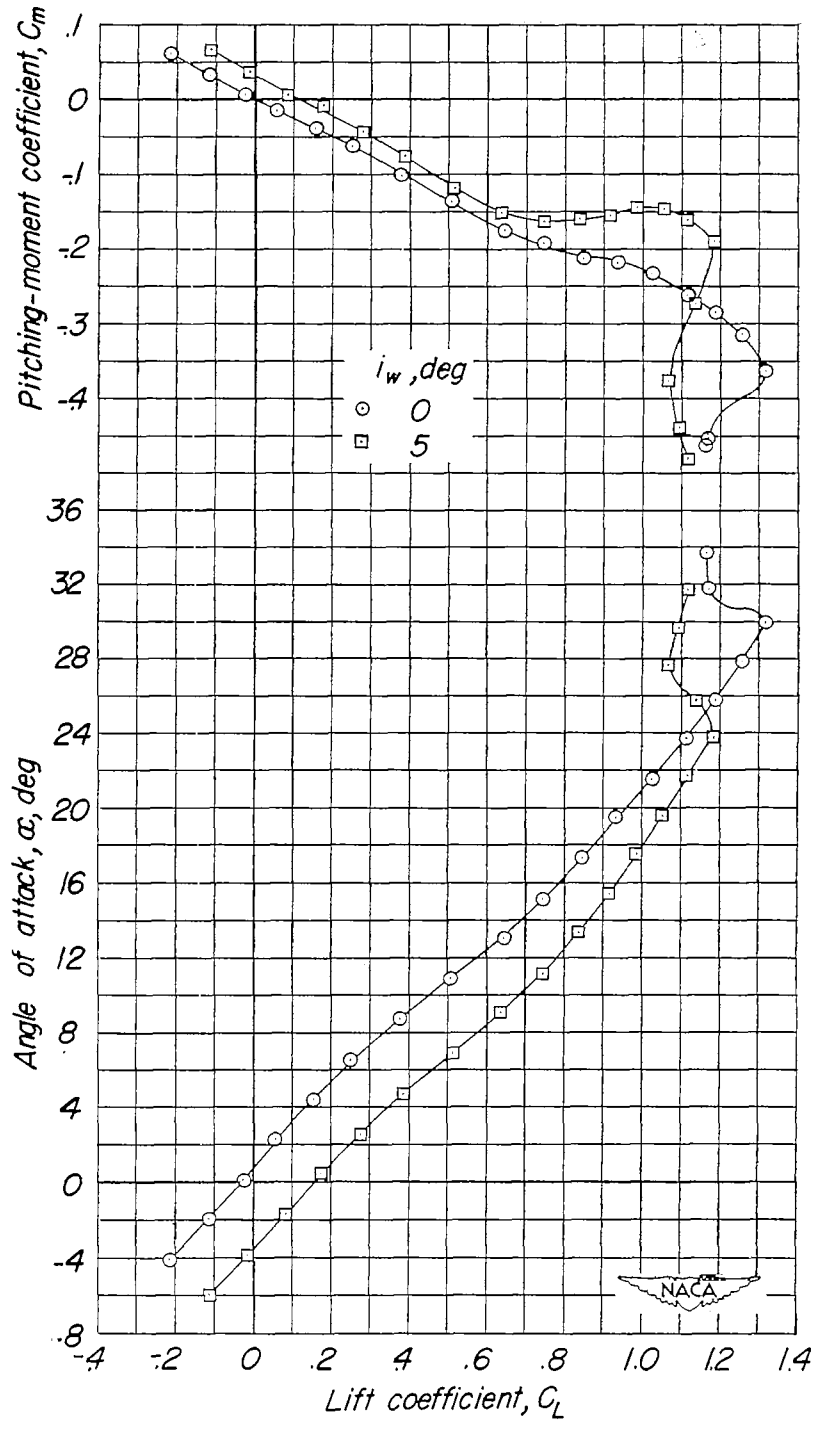

Figure 19.- The effect of wing incidence on the aerodynamic characteristics of the test model. $\Lambda = 60°$, $i_t = -\frac{3}{4}°$.

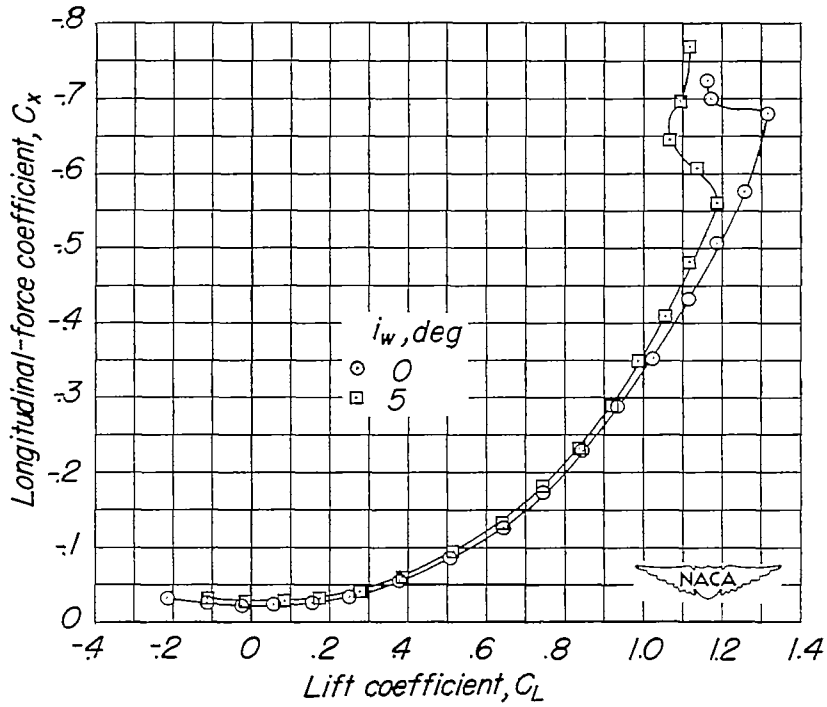

Figure 19.- Concluded.

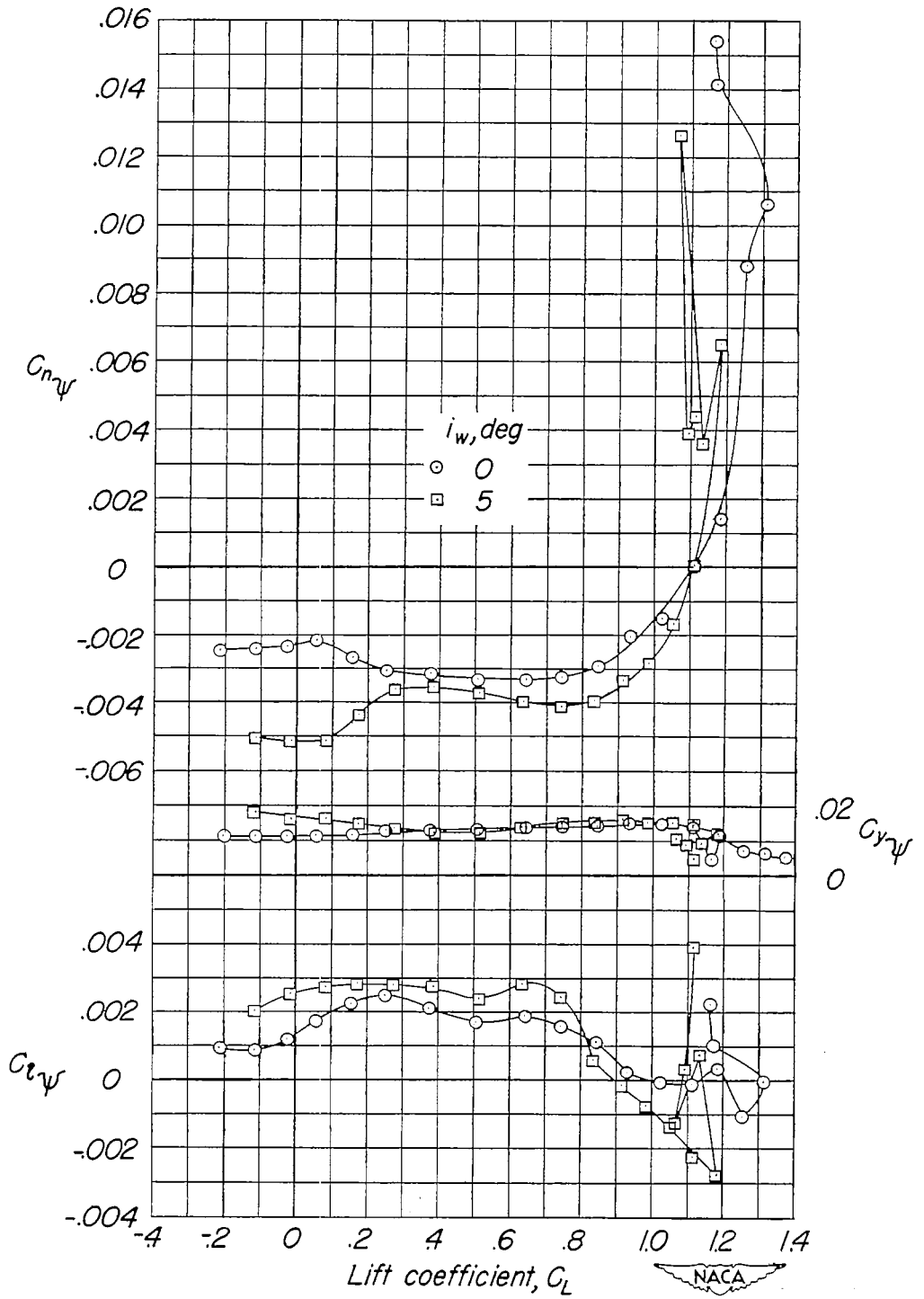

Figure 20.- The effect of wing incidence on the lateral-stability parameters of the test model. $\Lambda = 60°$, $i_t = -\frac{3}{4}°$.

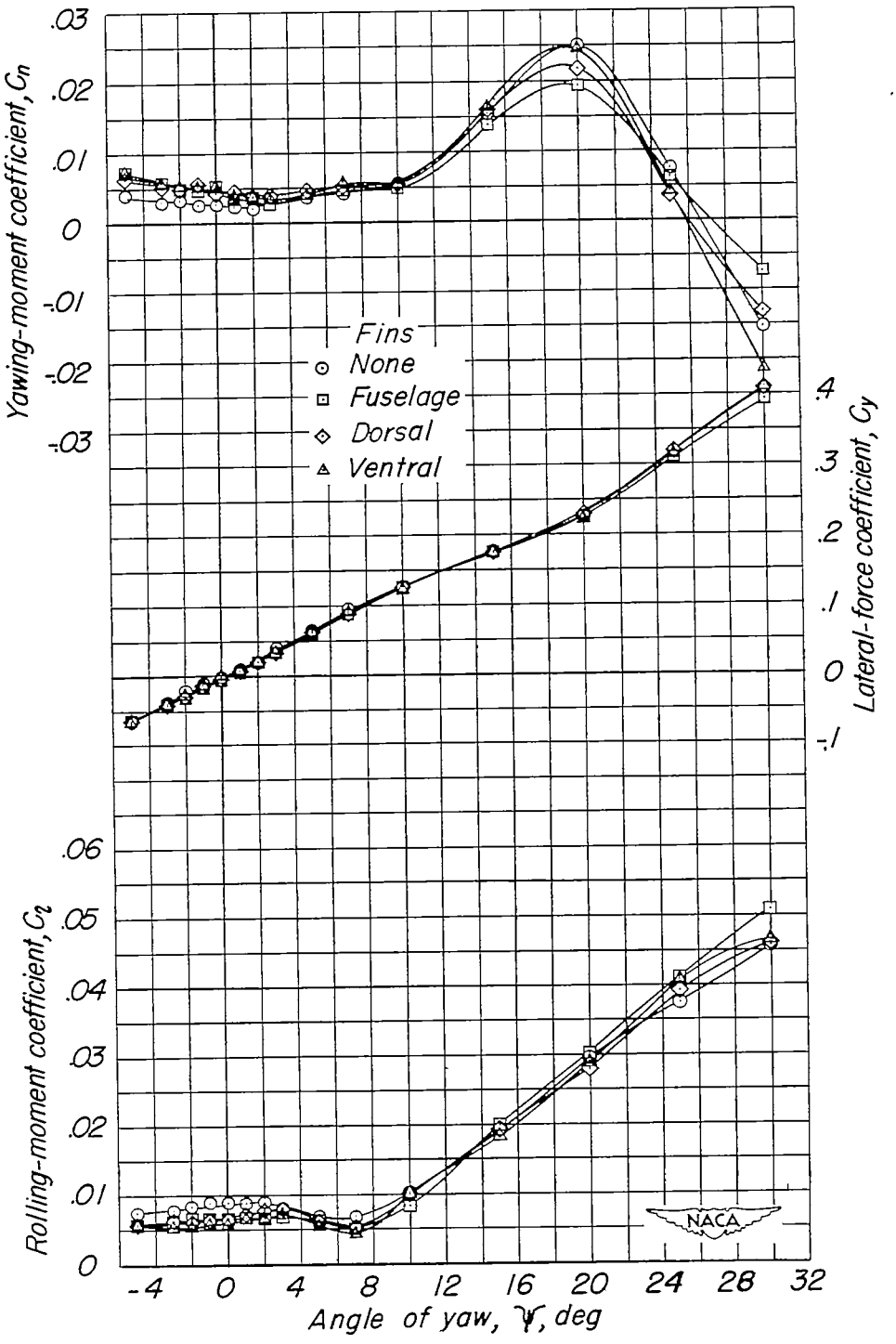

Figure 21.- The effect of various fuselage, dorsal, and ventral fins and a drooped horizontal tail on the aerodynamic characteristics in yaw of the test model. $\Lambda = 60^\circ$, $i_t = -\frac{3^\circ}{4}$, $\alpha = 23.66^\circ$.

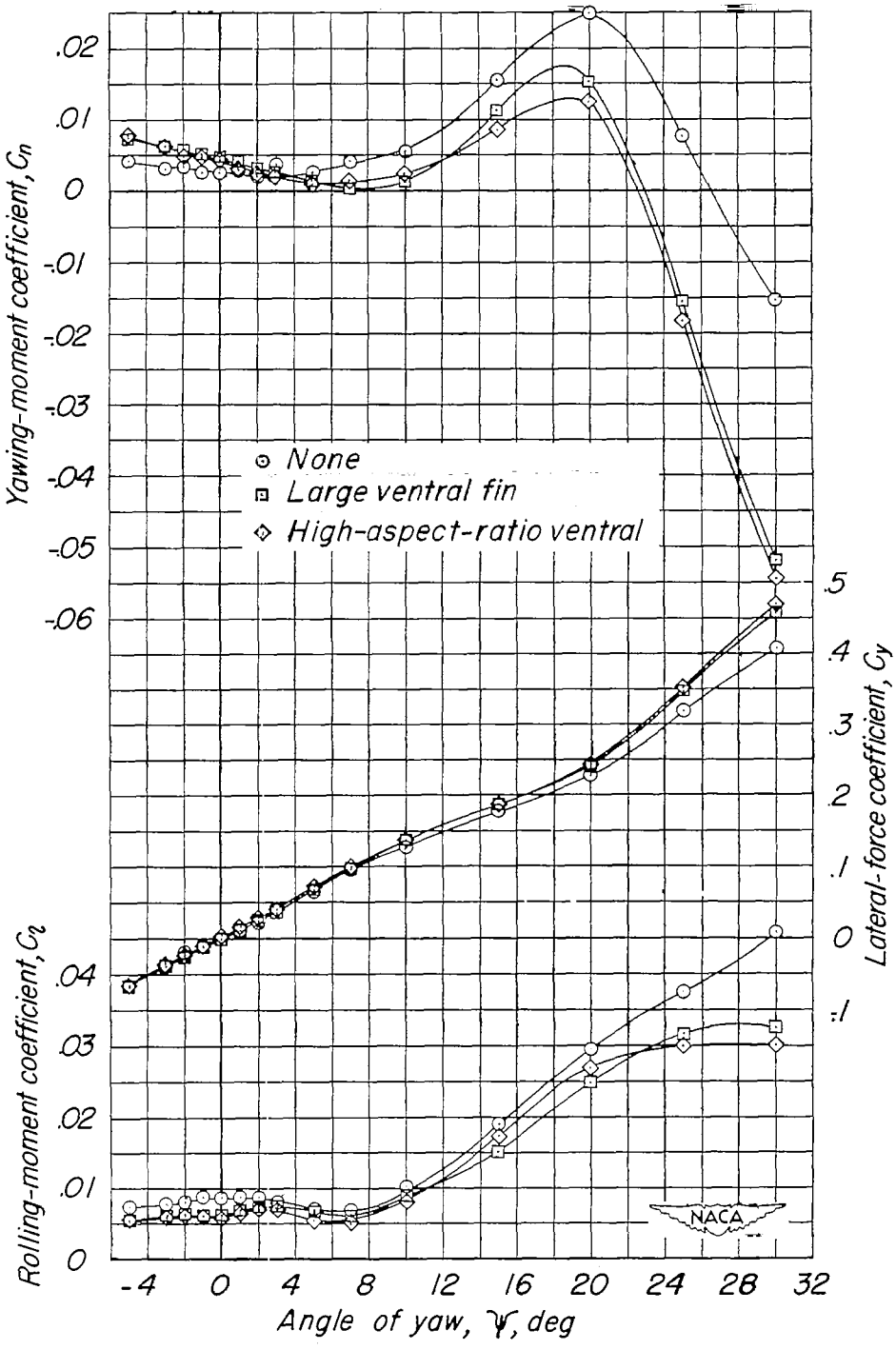

Figure 21.- Continued.

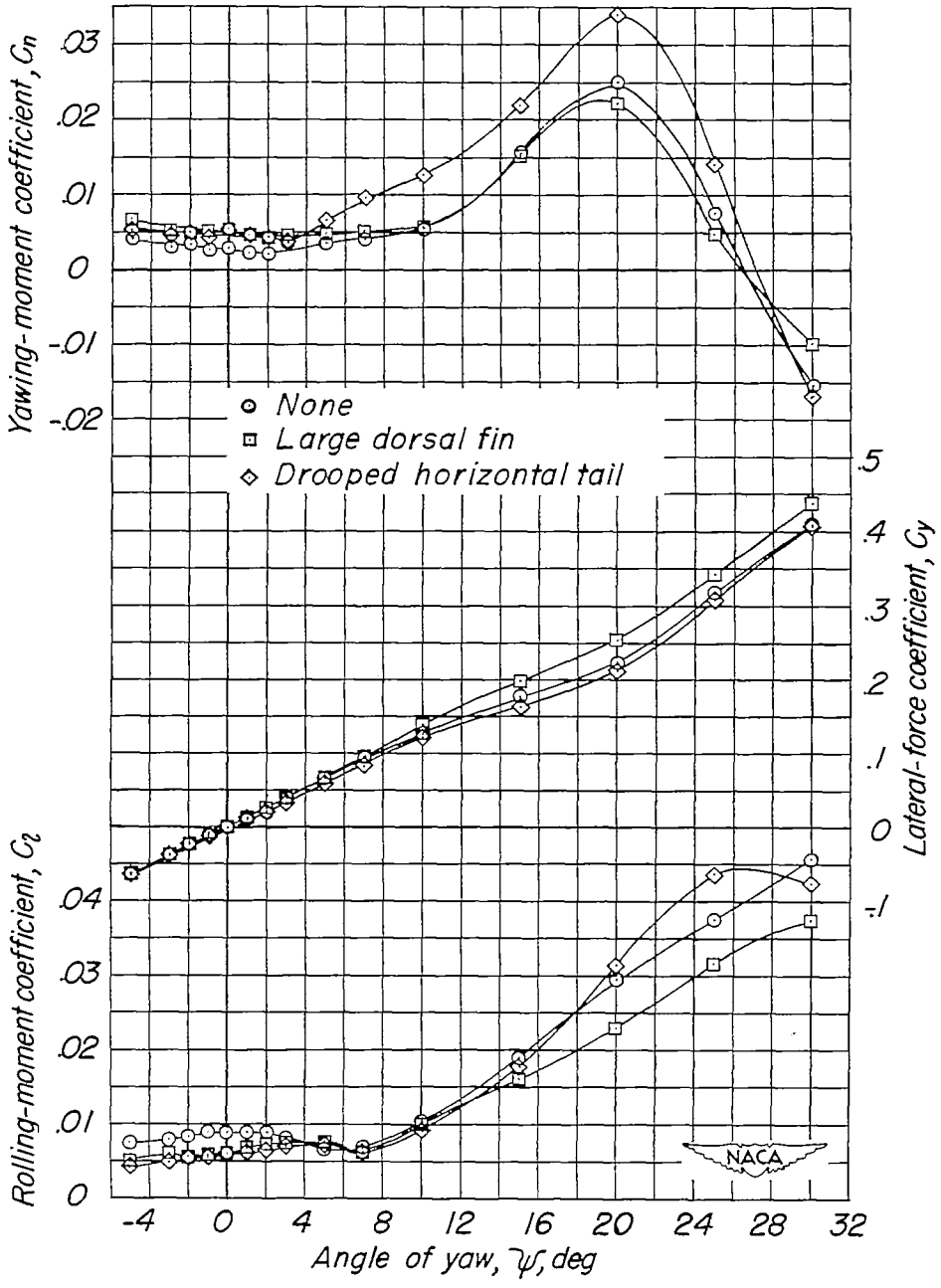

Figure 21.- Concluded.